

Performance and Joint Design of Co-existing Radar and Communications Systems

BY

NARUEPORN NARTASILPA
B.E., Kasetsart University, 2008
M.Sc., Florida International University, 2011

THESIS

Submitted as partial fulfillment of the requirements
for the degree of Doctor of Philosophy in Electrical and Computer Engineering
in the Graduate College of the
University of Illinois at Chicago, 2019

Chicago, Illinois

Defense Committee:

Natasha Devroye, Chair and Co-advisor
Daniela Tuninetti, Co-advisor
Besma Smida
Mojtaba Soltanalian
Jialing Liu, Huawei Technologies

Copyright by
Narueporn Nartasilpa
2019

The thesis is dedicated to my family, professors, and friends.

ACKNOWLEDGMENT

First and foremost, I would like to thank my Ph.D. advisors Professor Daniela Tuninetti and Professor Natasha Devroye for their dedications, encouragement and support during my Ph.D. years. Working with them to pursue my Ph.D. degree is my greatest honor. This dissertation and all my Ph.D. research would not have been done without their guidances and advices. Their enthusiasm in pursuing unexplored areas in academic research and their kindness have always inspired me. I will always be grateful to their mentoring and advising without any reservation.

I would also like to thank Professor Besma Smida, Professor Mojtaba Soltanalian, and Professor Erdem Koyuncu for their valuable time as well as their constructive comments and suggestions during my preliminary exam, which significantly contributed to this dissertation. Furthermore, I would like to thank Dr. Jialing Liu, who was my mentor during my 2018 summer internship at Huawei Technologies, for agreeing to be on my Ph.D. defense committee.

While doing research in the NICEST (Network, Information, Communications, and Engineering Systems), I have made incredible lab mates, who not only helped me through research discussions but also offered help and encouraged me through my tough times. Special thanks to Kenneth Palacio-Baus and Tang Liu. During my Ph.D. study, I also have been fortunate enough to make many friends whom made my Ph.D. life enjoyable and less stressful. I wish them the best in pursuing their current studies and future careers.

Last but not least, I would like to thank my family for everything they have done for me to raise me up to the way I currently am. Their endless love and unconditional support has given me many priceless

ACKNOWLEDGMENT (Continued)

experiences and opportunities. I have been blessed to be part of such a warm, wonderful, and supportive family that gives me freedom to pursue my life in every aspect with full support and understanding.

NN

CONTRIBUTION OF AUTHORS

The contents of this thesis is the result of a joint effort between my PhD advisors Professor Daniela Tuninetti, Professor Natasha Devroye and I. Our main contributions and a detailed list of prior existing work are presented in Chapter 1. The main results of our collaboration are found in Chapters 2, 3 and 4. Conclusions are finally summarized in Chapter 5.

Motivated by the problem of spectrum scarcity, we consider allowing a wireless communications system to share the underutilized spectrum with a radar system. Thus, interference between the co-existing systems are unavoidable. More precisely, we study and analyze how each system affects the performance of one another so as to use these insights as a guide to efficient co-design synergies. We make progress by providing an in-depth analysis of a single-carrier communications system suffering from weak, intermediate, and strong radar interference including system model, detection schemes, and error performances as well as optimizing a two-dimensional signal constellation that either maximizes the transmission rate or minimize the error rate. We further analyze and give comprehensive numerical evaluations of the error rate a more commonly-used multi-carrier OFDM communications system where various (optimal and suboptimal) decoders are presented. Lastly, the receiver operating characteristic of the radar system was investigated where we derive two detectors. Simulations results are then verified and conclusions are drawn.

TABLE OF CONTENTS

<u>CHAPTER</u>	<u>PAGE</u>
1 INTRODUCTION	1
1.1 Single-Carrier Communication System with Radar Interference	6
1.2 Multi-Carrier Communication System with Radar Interference	8
1.3 Radar System with Communications Interference	10
 2 A SINGLE-CARRIER COMMUNICATIONS SYSTEM SUFFERING FROM RADAR INTERFERENCE	 12
2.1 System Model	13
2.2 Detection Schemes	14
2.3 Decoding Regions	16
2.4 Symbol Error Rate (SER) Analysis	19
2.4.1 Pulse-Amplitude Modulation (PAM)	21
2.4.2 Square Quadrature Amplitude Modulation (Square-QAM)	21
2.4.3 Phase-Shift Keying (PSK)	22
2.5 SER Performance Evaluations	23
2.6 Signal Constellation Design	25
2.6.1 Optimization Formulation for Maximizing the Transmission Rates . .	25
2.6.2 Optimization Formulation for Minimizing the Error Rates	26
2.6.3 Optimization Results for Constellations with Maximal Rates	27
2.6.4 Optimization Results for Constellations with Minimum Error Rates .	30
2.6.5 Performance Comparison	32
2.7 Conclusion	34
 3 A MULTI-CARRIER COMMUNICATIONS SYSTEM SUFFERING FROM RADAR INTERFERENCE	 36
3.1 System Model	36
3.2 Detection Schemes	42
3.2.1 Optimal ML Decoder	43
3.2.2 Suboptimal Time-Correlated Decoder	43
3.2.3 Suboptimal Frequency-Correlated Decoder	44
3.2.4 Suboptimal Uncorrelated Decoder	45
3.3 Error Rate Analysis	46
3.4 Error Rate Performances of the Decoders	48
3.5 Conclusion	51
 4 A RADAR SYSTEM SUFFERING FROM COMMUNICATIONS INTER- FERENCE	 52

TABLE OF CONTENTS (Continued)

<u>CHAPTER</u>		<u>PAGE</u>
4.1	System Model	52
4.2	Hypothesis Testing	55
4.2.1	Case 1: Known Communications Constellation and Channel Gain . .	55
4.2.2	Case 2: Known Communications Channel Gain but Unknown Con- stellation	57
4.2.3	Case 3: Unknown Communications Constellation and Channel Gain .	58
4.2.4	Unaltered radar receiver	59
4.3	Receiver Operating Characteristic (ROC) Performance	60
4.4	Conclusion	65
5	CONCLUSION	67
6	FUTURE DIRECTIONS	71
6.1	Joint Bayesian Estimate	72
6.2	Two-step Decoding Process	72
6.2.1	Communications First, Radar Next	73
6.2.2	Radar First, Communications Next	74
	APPENDICES	76
	CITED LITERATURE	85
	VITA	91

LIST OF TABLES

<u>TABLE</u>		<u>PAGE</u>
I	THE OPTIMAL AND SUBOPTIMAL IC DECODING REGIONS FOR 8-PSK AT $S_{dB} = 10$ IN DIFFERENT REGIMES.	18
II	DESIGNED CONSTELLATIONS WITH MAXIMUM TRANSMISSION RATES AT VARIOUS S_{dB} AND $I_{dB} = 0.25S_{dB}$	28
III	DESIGNED CONSTELLATIONS WITH MAXIMUM TRANSMISSION RATES AT VARIOUS S_{dB} AND $I_{dB} = 2S_{dB}$	29
IV	DESIGNED CONSTELLATIONS WITH MINIMUM SER AT $S_{dB} = 20$ AND $I_{dB} \cong 0.25S_{dB}$, S_{dB} AND $2S_{dB}$ FOR $M = 4, 8,$ AND 16	31
V	COMPARISON OF MAXIMUM M FOR DIFFERENT CONSTELLATIONS FOR $\varepsilon = 10^{-1}$	32
VI	ERROR RATE (IN LOG-SCALE) COMPARISON OF THE RECEIVERS AT VARIOUS NUMBER OF SUBCARRIERS N , NUMBER OF OFDM BLOCKS L , AND RADAR PULSE WIDTH IN SAMPLES n_w	49

LIST OF FIGURES

<u>FIGURE</u>		<u>PAGE</u>
1	Decoding regions for $S = 10$ dB and $l = 15$ dB, and SER for $S = 10$ dB vs. l in dB.	24
2	SER Comparison for $M = 16$ and $S = 20$ dB.	33
3	ROC for a fixed pair $(h_r ^2, h_c ^2) = (S_r, S_c)$ where $S_r = 10$ dB and $S_c = \{0, 10, 20\}$ dB.	60
4	ROC for a fixed pair $(h_r ^2, h_c ^2) = (S_r, S_c)$ where $S_r = 10$ dB and $S_c = \{0, 10, 20\}$ dB with $\mathcal{X}_c = \{\emptyset, 4QAM, 16QAM\}$	61
5	ROC for a fixed $ h_r ^2 = S_r$ and a random $h_c \sim \mathcal{N}_{\mathbb{C}}(0, 10$ dB) with $ \mathcal{X}_c = \{\emptyset, 4QAM, 16QAM\}$	63
6	ROC for a fixed $ h_r ^2 = S_r$ and a random $h_c \sim \mathcal{N}_{\mathbb{C}}(0, 15$ dB) with $ \mathcal{X}_c = \{\emptyset, 4QAM, 16QAM\}$	63
7	SER comparison vs. S_{dB} for various M values.	84

SUMMARY

Spectrum sharing between radar and communications systems has been a topic of interest as a novel solution to the increasing demand for new wireless services but limited available bandwidth. In particular, the S-band (2-4 GHz) is one of the potential candidate bands for spectrum sharing as it is where radar systems (e.g., air traffic control, Navy surveillance, and weather), communications satellites, and commercial wireless networks (e.g., WiFi and Long-Term Evolution (LTE)) operate. Therefore, a good understanding of how current radar and communications systems affect one another is essential to efficiently co-design both systems to operate reliably (without performance degradation ideally).

The main focus of this work is to attempt an analytical characterization of the optimal performance of an uncoded communications system, using complex-valued modulation schemes when the optimal Maximum Likelihood (ML) detector is used, in the presence of an unaltered radar system. To do so, we need a tractable model. Radar systems periodically transmit radar pulses of large amplitude and short duration while communications systems send signals of significantly lower power, smaller bandwidth, and 100% duty-cycle. This implies that each narrowband subcarrier in an Orthogonal Frequency Division Multiplexing (OFDM) communications system experiences the radar interference as an approximately amplitude-constant additive interference. This amplitude can be accurately estimated from the knowledge of the (slowly varying) parameters of the radar waveform and the relative geometry between the radar transmitter and the communications receiver. The phase however changes very rapidly due to multi-path propagation; the worst case scenario is when such a random phase is uniformly distributed. With these considerations in mind, we build a simple model for when a radar and a communications

SUMMARY (Continued)

system operate in the same frequency band, which captures some key performance bottlenecks and highlights different operating regimes.

A simplified single-carrier communications system with additive radar interference and Gaussian noise is first considered and the constellation design with the goal of maximizing the transmission rates subject to average power and error rate constraints, and minimizing the error rates under a power budget are later proposed. Two regimes, where the radar interference power, measured by the Interference-to-Noise ratio (INR), is low and very high compared with the intended communications signal power, measured by the Signal-to-Noise ratio (SNR), are thoroughly investigated and the Symbol Error Rate (SER) expressions for both regimes are presented. In the weak radar interference regime, the radar interference is treated as Gaussian noise and the probability of error increases with the radar power. At low INR, the channel behaves as a complex-valued AWGN channel and the designed constellations exhibit a concentric (almost equilateral) hexagonal structure as the number of signal points increases. In the very strong radar interference regime, the radar interference can be estimated and subtracted off the received signal at the cost of cancelling out a portion of the communications signal, which reduces the effective SNR at the receiver, and the probability of error exhibits an irreducible error floor that can be exactly characterized. At high INR, the channel behaves as a real-valued phase-fading AWGN channel and the designed constellations are shaped as an unequally-spaced Pulse-Amplitude Modulation (PAM). In the intermediate radar interference regime, where the radar and communications signals are received at roughly the same strength, the probability of error attains its maximum value, and it is numerically shown that the hexagon-shaped constellation transitions into an unevenly PAM-shaped as the radar power increases.

SUMMARY (Continued)

Next, the interference caused by a radar system on a multi-carrier OFDM-based communications receiver is investigated. Due to the unknown time delay between the communications and radar signals at the OFDM receiver, the received signal becomes correlated over time and across carriers. The performance of the optimal ML decoder, which considers both time and frequency correlation for the OFDM system, is measured in terms of error rates and numerical results show that a suboptimal time-correlated decoder is slightly inferior to the optimal ML decoder but outperforms symbol-by-symbol and frequency-correlated suboptimal decoders.

Finally, we investigate the complimentary problem, where a radar system is interfered by a communications signal, and its Receiver Operating Characteristic (ROC) performances for two composite hypothesis testings, the Average Likelihood Ratio Test (ALRT) and the Generalized Likelihood Ratio Test (GLRT), are derived. Certain knowledge of communications system parameters is assumed to be available at the radar receiver. Specifically, the radar receiver knows the set of all possible communications symbols but not the actual transmitted symbol. Three scenarios are considered here: the communications constellation and the channel gain between the communications transmitter and the radar receiver are either known or unknown. When both the communications constellation size and the channel gain are known, it is shown that a communications interference of sufficiently low power slightly degrades the radar detection performance, and as the interference power becomes stronger than the radar power, the radar receiver can successfully decode and cancel the communications symbol where the ROC curve approaches the no interference case; the GLRT detector is shown to very well capture the the performance of the ALRT detector. When the channel gain is known, it is shown that the optimal ALRT detector can either ignore or cancel the communications interference for weak or strong

SUMMARY (Continued)

interference power, respectively; the GLRT is shown to well approximate the ALRT in the weak regime but not in the strong regime, with the largest gap from the ALRT in the intermediate interference regime. Interestingly, for the scenario where the radar receiver has no knowledge of the channel gain from the communications transmitter, the GLRT detector does not depend on the received signal, which yields a straight line in the ROC curve no matter what the power of the radar signal is; hence, the GLRT is not suitable in this scenario. For all cases, simulations confirm that the ALRT performance improves with more knowledge of the communications parameters, as expected.

CHAPTER 1

INTRODUCTION

With an ever growing number of wireless services, the need for extra bandwidth has become a serious issue for the wireless communications industry. One solution to the increasing demand for spectral resources of wireless services is to allow the wireless communications systems to utilize the radar spectrum, sparking much research in both the radar and communications communities. For instance, DARPA (Defense Advanced Research Projects Agency) has launched the SSPARC (Shared Spectrum Access for Radar and Communications) program to encourage research in this direction [1] and the NSF (National Science Foundation) also has a dedicated crosscutting program for EARS (Enhancing Access to the Radio Spectrum) [2]. The spectrum of interest for sharing is the S-band (2-4 GHz), where several wireless communications systems (i.e., Wi-Fi and WLAN) and radar systems (i.e., air surveillance and weather) operate. The economical implications of successful spectrum sharing, as well as the technical challenges of maintaining integrity under spectrum sharing for each individual system, are difficult to understate. Therefore, novel solutions for the efficient and fair sharing of the spectrum is needed.

The interference effects between communications and radar systems were already considered in the 50s [3], but have only recently come to the forefront due to the significant increase of wireless services for smartphones, tablets and real-time video streaming. Much recent work has looked at issues related to the co-existence between radar and communications systems. The feasibility of dynamic spectrum sharing between wireless communications systems and air traffic control radar is investigated in [4] via a numerical simulation. The effect of a rotating radar on bit and packet error rates of a WiMax receiver

was simulated in [5]. In [6, 7], the authors venture into the theoretical analysis that looks at a tradeoff between communications information rate and radar estimation rate.

The longer term goal for spectrum sharing may be to modify radar and communications systems to co-exist ([8] and references therein). However, to effectively design co-existence systems, it is important to first understand the impact of unaltered systems on one another. In this vein, there are two important avenues to visit: how communications signals affect the performance of radar systems, and the reverse: how radar signals affect the error rate (and other metrics) of communications systems. The following list is a very small extract of the available literature considering the former aspect. The authors in [9] studied the effects of amplitude and frequency modulated audio signals on radar system and concluded that the FM interference behaves like AWGN but AM/DSB interference behaves quite differently. A cognitive design of the transmit signal and receive filter optimizing the radar detection performance by inducing spectral constraints on the radar waveform to predict the actual scattering scenario and to acquire information about hostile active jammers was proposed in [10]. National Telecommunications and Information Administration (NTIA) carried out an experimental analysis of interference of digital signals on radars, which showed that the interference to noise ratio as low as -6 to -9 dB significantly degrades the radar performance [11, 12].

While there have been many numerical and experimental studies on the loss of performance of the radar and communications systems once they co-exist [13–17], there has not been much research on analytical models and analysis using such models to demonstrate the effect of unaltered radar interference on the error rate performance of the communications systems despite its relevance for designing more backwards-compatible spectrum sharing solutions. Herein, our research is mainly focused on analyti-

cally characterizing the impact of unaltered radar interference on wireless communications systems as a starting point for a practical interference management approach. In [18], we investigated the effect of radar interference on an uncoded *real-valued* modulation scheme used on an Additive White Gaussian Noise (AWGN) channel and then extended our closed-form analysis of the average SER to any *complex-valued* modulation scheme in [19]. We explicitly consider commonly-used PAM, QAM and PSK constellations but the results and insights are valid in general.

How to enable the communications and radar systems to co-exist in an efficient manner can be approached from several angles. One straightforward solution is to split the available resources (in time or frequency) through policy so that each system operates independently and interference is avoided altogether. For example, the authors in [20] proposed a time-frequency (carrier by carrier) resource allocation algorithm for co-existing LTE advanced cellular and S-band radar systems. Such resource allocation schemes lead to orthogonal resource allocation, quite different from the simultaneous, overlapping frequency spectrum sharing studied here. Another direction is to retrofit one system so as to better withstand the effect of the other system. Rather than retrofitting one system, one could opt to re-design and co-design both the communications and radar systems. In [21], it was concluded that a co-design is key in improving the performance of co-existing architectures, and co-designs have attracted much recent attention, see for example [22] and references therein. In contrast to the resource allocation (orthogonalizing) approach of [20], a framework for a joint radar-communications system was introduced in [23], where only one transmitted signal (decoupled into training and data portions) is used for simultaneous operations for both systems. The optimal training signals are shown to yield both the largest lower bound on the communications rate and the maximum probability of detection. The work

in [23] considered a scenario where both the radar and communications systems share a transmitter and receiver. Waveform design is another popular co-design scheme. This technique utilizes the characteristics of the other system's signal so as to improve each system's performance through carefully designing their transmitted waveforms [24–27]. The authors in [28–30] proposed a spectrum sharing algorithm between a Multiple-Input Multiple-Output (MIMO) radar and an LTE cellular system, in which the loss in radar performance is minimal when one selects the best channel onto which to null-project the radar signal so as to create minimal interference to the LTE system. In [31], an LTE packet scheduling algorithm based on channel sensing was proposed for spectrum allocation for an LTE system during radar intermittent periods resulting in a slight performance degradation for the LTE system. The experimental study of the degradation in performances of the coexisting air traffic control radar and LTE systems in the S-band in [32] reported that the LTE system in the TDD bands suffers a significant performance degradation when the radar pulses hit the synchronization packets, and discussed the improved filtering and spectrum sensing (among the possible mitigation techniques) for both systems. In [22], the authors looked at how to design the radar system so as to maximize the Signal-to-Interference-plus-Noise-Ratio (SINR) at the MIMO radar receiver subject to MIMO communications system requirements. Spectrum sharing between a communications system and a MIMO radar system modeled as MIMO interference channel is considered in [33], where a zero-forcing pre-coder for radar transmitter that completely eliminates the radar interference to communications users was proposed and the impact on both the radar and communications systems was investigated. In [34], the authors discussed the gray space spectrum sharing between a primary rotating radar and a secondary cellular device that allows the secondary device to transmit as long as its resulting interference does not exceed the radar's tolerable level with an

extension to multiple rotating radars and cellular network hotspots presented in [35]. In [36], the radar waveforms were optimized so as to maximize the radar estimation rate as well as the communications data rate. These co-design schemes differ from the presented scheme here, in which the radar system is left unaltered.

In general the focus has been mainly on the design of radar waveforms, or more generally the whole system structure of radar system, for enhanced spectral efficiency when co-existing with communications systems. In this work, we are interested in the complementary problem: the design of the communications signal constellation so as to optimize the communications system performance in the presence of a radar signal. Here, in contrast to other work, the radar signal is left unaltered.

Past work has studied the optimal constellation design under various performance metrics for different channel models. However, to the best of our knowledge, no one has looked at the channel model with additive radar interference considered here. For example, the optimization of complex signal constellations in the presence of Gaussian noise only was presented in [37], where the minimization of the probability of error was based on an asymptotic approximation of the ML decoder for large Signal-to-Noise-Ratio (SNR). Another example is [38] where the authors presented the optimal signal constellation for phase noise channels when using either the SER or the average mutual information for an ML detector as the optimization objectives.

Motivated by the necessity of delivering the largest possible rate subject to an error rate being below an application-dependent value while not exceeding a power budget, we studied the problem of maximizing the cardinality of the constellation subject to average constellation power and SER constraints [39]. The more common approach of minimizing the SER for a fixed constellation size subject

to an average power constraint is also investigated here. This problem is well motivated for cognitive networks in which the communications nodes are “intelligent” and may adapt their transmission to their sensed spectral environment. In particular, if they sense a radar signal, depending on its strength, they may adapt their constellation and decoding schemes as proposed here.

While there have been many studies on how radar and communications systems can co-exist within tolerable performance degradation, clear insights on how unaltered radar and communications systems affect one another has not been investigated much despite its relevance to better determine which technology should be pursued for reliable radar-communications coexistence. Herein, our research is mainly focused on the performance of a communications receiver with interference from unaltered radar signals. The findings of this work are relevant for systems where changing the hardware may be too costly, but further digital signal processing of the baseband received signal is viable.

This paper investigates the effect of radar interference on two types of communications systems: a single-carrier, and a multi-carrier communications system.

1.1 Single-Carrier Communication System with Radar Interference

In Chapter 2, we consider a transmitter wishing to communicate with a receiver over a memoryless additive noise channel, where the noise consists of a Gaussian component and a radar interference. The radar interference is modeled as having a known constant amplitude and a known random phase uniformly distributed in $[0, 2\pi]$. We seek to understand how the SER of an uncoded communications system using a complex-valued modulation scheme is affected by a specific model of radar interference under a range of low to high level of radar power relative to the SNR of the communications signal. Based on the obtained SER expressions, we aim to design a constellation that maximizes the transmis-

sion rate, measured by the number of signal constellation points, subject to the average power and error rate not exceeding predetermined values as well as the ‘dual’ problem of the constellation design that minimizes the SER subject to a fixed rate since many widely-used complex-valued modulation schemes, such as QAM and PSK, are not necessarily optimal for this radar-interfered channel.

We observe three different regimes of operation depending on the relative value of the radar interference power, measured by the INR, and the intended signal power, measured by the SNR:

1. *Treat interference as Gaussian noise*: when $\text{INR} \leq \text{SNR}$, we show that it is optimal to use the classical minimum distance decoder as if the overall channel noise were Gaussian. As expected, the SER is minimal when $\text{INR} = 0$ and it increases with INR. The channel behaves as a complex-valued AWGN channel and our optimization results show that the designed constellation is approximately shaped as a concentric hexagonal lattice. More precisely, the constellation points are the vertices of a trellis of almost equilateral triangles that form concentric almost equilateral hexagons as the number of signal points increases. We shall refer to this shape as ‘hexagonal-like’.
2. *Interference cancellation*: when $\text{INR} \gg \text{SNR}$, we show that it is optimal to estimate the phase of the radar interference (as the phase of the received signal) and subtract its contribution from the received signal at the communications receiver. Interestingly, in the process of canceling the radar interference, part of the useful signal is also cancelled. This in turn reduces the effective SNR at the communications receiver and thus the SER exhibits an irreducible error floor that does not coincide with the case $\text{INR} = 0$. This error floor can be exactly characterized as the attainable SER over a narrowband fading channel with multiplicative fading that is perfectly known at the receiver but unknown at the transmitter. The channel behaves as a real-valued phase-fading

AWGN channel, indicating a loss of one of the two real-valued dimensions, and our optimization results show that the designed constellation is approximately shaped as an unevenly-spaced PAM. More precisely, the constellation aligns all the points on an almost-straight line with the largest possible minimum distances. We shall refer to this shape as ‘PAM-like’.

3. *Intermediate regime*: this regime represents the worst operating point from the perspective of a communications system coexisting with a radar system as the SER attains its highest value. Depending on the SNR, modulation scheme and constellation size, we heuristically observe that the highest SER takes place around $\text{INR} \cong \text{SNR}$. Thus, an exhaustive search for the INRs is required to properly design a constellation. Our optimization results show that the designed constellation stretches from a hexagonal-like constellation at low INR to a PAM-like one at high INR.

These intuitions and the observed three operating regimes are confirmed to be fundamental by the recent information theoretic analysis [40] of the Shannon’s capacity (i.e., largest possible coded rate that can be reliably decoded) for the considered channel model.

1.2 Multi-Carrier Communication System with Radar Interference

We conduct a comprehensive analysis of a discrete-time channel model for an OFDM-based multi-carrier communications system experiencing radar interference in Chapter 3. We are interested in studying the performance of this particular model in terms of block and symbol error rates. Due to the unknown time lag between communications and radar signals at the OFDM receiver, the received signal becomes correlated among OFDM symbols (time) and across subcarriers (frequency). By evaluating the error rate performances of the ML decoders under various OFDM and radar systems parameters via simulations, we observe that the optimal frequency-time-correlated receiver is the best as expected and

that the suboptimal time-correlated receiver, which is slightly inferior to the the optimal receiver, outperforms the suboptimal frequency-correlated and the worst performing symbol-by-symbol receivers.

The performance limits of such a communication system co-existing with an interfering radar system were explored in [41], where it was concluded that 1) the average error rate of a communications system increases with increasing radar interference power up to the point where both the signal and interference have approximately the same power levels, and then it decreases to an asymptote that can be exactly characterized, and 2) the probabilities of detection and false alarm increase with the (non-Gaussian) communications interference power for a fixed-threshold detector, while the detection probability decreases with increasing communications power but the false alarm probability either decreases or remains roughly constant for a cell-averaging adaptive-threshold radar detector.

Next, the complimentary problem where the performance of a radar system suffering from communications interference is analyzed. While it is common to model the wireless communication interference at a radar receiver as a Gaussian process, it has been found in [42] that interference from a communications system affects the radar detection does not behave like Gaussian interference. This finding is further supported by the study of the impact of an interfering 4G communications signal radar systems in the L- and S-band [43]. A non-Gaussian statistical model of the communications interference under path loss and Rayleigh fading based on an empirical approach was proposed in [44].

The Receiver Operating Characteristic (ROC) performance of the Average Likelihood Ratio Test (ALRT) and the Generalized Likelihood Ratio Test (GLRT) were investigated in [45] where closed-form expressions for these two tests were obtained based on the Gaussian assumption.

1.3 Radar System with Communications Interference

In Chapter 4, the radar system is interested in detecting whether a target is present or absent at a specific location in the presence of communications interference as measured by the ROC curve. The communications interference is assumed to come from a discrete constellation. Certain knowledge of communications system parameters is assumed to be available at the radar receiver. Specifically, the radar receiver knows the set of all possible communications symbols (all possible constellation points) but not the actual transmitted symbol. The following three scenarios are considered based on the availability of the channel gain between the communications transmitter and the radar receiver and the communications constellation used:

1. The communications constellation and the channel gain are fixed (and thus known) at the radar receiver.
2. The channel gain is fixed (and thus known) at the radar receiver but the communications constellation is not. This is because the communications transmitter adapts its transmission based on the channel gain to its communications receiver.
3. Both the communication constellation and the channel gain are unknown at the radar receiver. Here we also assume that the constellation is changed by the communications transmitter so as to adapt to the channel gain to its communications receiver as in Scenario 2 and that the channel gain is Rayleigh distributed and independent of the communications constellation.

We derive ROC curves based on the Bayesian approach (also referred to as the ALRT test), where prior knowledge of the unknown parameters is required [46]. We find that a communications interfer-

ence of sufficiently low power slightly degrades the radar detection performance and the probability of detection decreases with increasing communications power. As the interference power becomes stronger than the radar power, the optimal radar receiver can successfully decode and cancel the communications symbol, and the ROC curve approaches the no interference case.

Another composite hypothesis testing approach based on the maximum likelihood estimation of the unknown parameters (referred to as the GLRT test) is also investigated and its performance is compared with the aforementioned ALRT test. For the first and second scenarios, the ALRT and GLRT demonstrate a similar performance when the communications power is either sufficiently low or high. In the third scenario, the GLRT performance deteriorates as it does not depend on the received signal or the interfering communications symbol.

CHAPTER 2

A SINGLE-CARRIER COMMUNICATIONS SYSTEM SUFFERING FROM RADAR INTERFERENCE

(This chapter was previously published as “Let’s share CommRad: effect of radar interference on an uncoded data communications system”, in *Proceedings of IEEE Radar Conference (RadarConf)* [18], “On the Error Rate of a Communication System Suffering from Additive Radar Interference”, in *Proceedings of IEEE Global Communication Conference (GlobeCom)* [19], and “Signal Constellation Design in the Presence of Radar Interference and Gaussain Noise”, in *Proceedings of IEEE Military Communications Conference (MILCOM)* [39].)

First we look at a single-carrier communications system affected by a radar interference, which is a special case of a more complicated OFDM-cased multi-carrier communications system discussed in Chapter 3.

In this chapter, we analytically derive the optimal detection scheme then present the symbol error rate expressions for various optimal and suboptimal ML decoders. Finally, we design signal constellations for two different optimization problems: one is to maximize the transmission rate under a certain power budget and an error rate constraint, while the other is to minimize the probability of error under a certain power constraint and a fixed rate condition.

2.1 System Model

Radar systems periodically transmit pulses of large amplitude¹ and short duration, while communications systems generally send signals of significantly lower power, smaller bandwidth, and 100% duty-cycle. This implies that a narrowband communications system experiences the radar interference as an approximately amplitude-constant additive signal. This amplitude can be accurately estimated by, for example, listening periodically to the channel for some time prior to transmission, which is doable because of the slowly varying parameters of the radar system. The phase shift, on the other hand, is from the multiplication of the radar carrier frequency by the radar pulse propagation delay; even a small variation in propagation delay causes a large phase difference, which may be difficult to track; for this reason and similar to well accepted fading models [48], the phase is assumed unknown and uniformly distributed on $[0, 2\pi]$. This assumption is consistent with [49], which shows that the joint Probability Mass Function (PMF) of the radar amplitude and phase consists of a union of multiple constant amplitude, uniform phase pieces. In other words, for several amplitudes, the joint PMF is uniformly distributed across the phase (for a given amplitude). One of the amplitudes clearly dominates the others, and hence the radar signal's joint PMF can be approximated by a phase uniform in $[0, 2\pi]$ at the given dominant amplitude. In the following single-carrier system, we thus approximate the radar interference at a communications receiver as an additive signal with a known (dominant) amplitude, which (by assumption) may be estimated due to the radar signal's high power, and uniformly distributed phase,

¹Since the radar power is significantly higher than the communications power, the analog-to-digital converter at the communications receiver might not see the small communications signal. This may be an issue in practice, but can be mitigated [47]. Note that mitigating this effect is not the focus of this work.

which is assumed to be unknown and changing from one channel use to another. The correlations in the received signal at an OFDM receiver, caused by the unknown time lag between arriving communications and radar signals, will be presented in Chapter 3.

The discrete-time complex-valued received signal at the single-carrier communications receiver is

$$Y = \sqrt{S}X + \sqrt{I}e^{j\Theta} + Z, \quad (2.1)$$

where X is the transmitted symbol from the constellation $\mathcal{X} = \{x_1, \dots, x_M\}$ of unit energy and equally likely points, Θ is the radar phase uniform in $[0, 2\pi]$, and Z is a zero-mean unit-variance proper-complex Gaussian noise. Here we assume that the random variables (X, Θ, Z) are mutually independent. S denotes the average Signal-to-Noise Ratio (SNR) of the communications signal, while I denotes the average Interference-to-Noise Ratio (INR) of the radar signal. The pair (S, I) is assumed known and fixed at the receiver.

2.2 Detection Schemes

Based on the system model in Equation 2.1, the channel conditional distribution for the received signal $Y = y \in \mathbb{C}$ at the single-carrier communications receiver is given by

$$f_{Y|X,\Theta}(y|x, \theta) := \frac{1}{\pi} e^{-|y - \sqrt{S}x - \sqrt{I}e^{j\theta}|^2}.$$

The optimal ML receiver chooses an estimate of the transmitted symbol $x_\ell \in \mathbb{C}$

$$\hat{\ell}^{(\text{OPT})}(\mathbf{y}) = \arg \max_{\ell \in [1:M]} \mathbb{E}_{\Theta} [f_{Y|X,\Theta}(y|x_\ell, \Theta)]$$

$$\begin{aligned}
&= \arg \min_{\ell \in [1:M]} \left(|y - \sqrt{S}x_\ell|^2 - \ln \mathbb{E}_\Theta [e^{2\Re\{(y - \sqrt{S}x_\ell)\sqrt{I}e^{-j\Theta}\}}] \right) \\
&= \arg \min_{\ell \in [1:M]} \left(|y - \sqrt{S}x_\ell|^2 - \ln I_0(2\sqrt{I}|y - \sqrt{S}x_\ell|) \right), \tag{2.2}
\end{aligned}$$

where I_0 denotes the modified Bessel function of the first kind of order zero [50, eq(9.6.16)].

We thoroughly investigate two regimes: weak radar interference when the INR of the radar signal is smaller the SNR of the communications signal, and very strong radar interference for the opposite.

Low INR regime: When $I \ll S$, the term $I_0(z) \cong 1$ in Equation 2.2 for $|z| \ll 1$ [50, eq(9.6.12)]. As a result, the optimal ML receiver can be approximated as

$$\hat{\ell}^{(\text{OPT})}(\mathbf{y}) \approx \hat{\ell}^{(\text{TIN})}(\mathbf{y}) = \arg \min_{\ell \in [1:M]} |y - \sqrt{S}x_\ell|^2. \tag{2.3}$$

We can see that the decoder at low INR is actually the minimum Euclidean distance decoder implying that the radar interference is treated as Gaussian noise. We refer to this decoder as the ‘TIN’ receiver, in which ‘TIN’ stands for Treat Interference as Noise.

High INR regime: When $I \gg S$, the term $I_0(z) \cong e^{|z|}$ in Equation 2.2 for $|z| \gg 1$ [50, eq(9.7.1)]. As a result, the optimal ML receiver can be approximated as (see Appendix B for detailed derivation)

$$\begin{aligned}
\hat{\ell}^{(\text{OPT})}(\mathbf{y}) &\approx \hat{\ell}^{(\text{IC})}(\mathbf{y}) = \arg \min_{\ell \in [1:M]} \left(|y - \sqrt{S}x_\ell - \sqrt{I}| \right)^2 \\
&= \arg \min_{\ell \in [1:M]} \left(\Re\{e^{-j\Theta}(y - \sqrt{I}e^{j\Theta} - \sqrt{S}x_\ell)\} \right)^2. \tag{2.4}
\end{aligned}$$

The expression in Equation 2.4 suggests that the radar interference can be estimated and subtracted off the received signal, but part of the communications signal is also removed. Thus, one of the two real-valued dimensions of the received signal is lost and the channel becomes the following real-valued phase-fading Gaussian channel

$$Y_{\text{eq}} = \Re\{e^{-j\Theta}\sqrt{\mathbf{S}}\mathbf{X}\} + Z_{\text{eq}}, \quad Z_{\text{eq}} \sim \mathcal{N}_{\mathbb{R}}(0, 1/2), \quad (2.5)$$

where the phase-fading $e^{-j\Theta}$ is known at the receiver but unknown at the transmitter. We refer to this decoder as the ‘IC’ receiver, in which ‘IC’ stands for Interference Cancellation.

2.3 Decoding Regions

In the preceding section, we presented the optimal and suboptimal detection schemes. Here we take a closer look at their decoding regions to get a better visualization of differences between having only Gaussian noise and having both Gaussian noise and radar interference.

The optimal ML receiver, based on Equation 2.2, prefers point x_ℓ to x_k if

$$|y - \sqrt{\mathbf{S}}x_\ell|^2 - \ln I_0(2\sqrt{I}|y - \sqrt{\mathbf{S}}x_\ell|) < |y - \sqrt{\mathbf{S}}x_k|^2 - \ln I_0(2\sqrt{I}|y - \sqrt{\mathbf{S}}x_k|).$$

Low INR regime: For $I \ll \mathbf{S}$, the TIN receiver prefers point x_ℓ to x_k if

$$|y - \sqrt{\mathbf{S}}x_\ell|^2 < |y - \sqrt{\mathbf{S}}x_k|^2.$$

In other words, the TIN receiver decodes x_ℓ if the received signal y is closer to x_ℓ than x_k . Thus, the TIN decoding regions depend only on the minimum distance as in the AWGN channel.

High INR regime: For $I \gg S$, the IC receiver prefers point x_ℓ to x_k if

$$\left(|y - \sqrt{S}x_\ell| - \sqrt{I}\right)^2 < \left(|y - \sqrt{S}x_k| - \sqrt{I}\right)^2. \quad (2.6)$$

The expression in Equation 2.6 can be separated into the following cases:

$$\begin{array}{l} \text{Case 1: } \left. \begin{array}{l} |y - \sqrt{S}x_\ell| > \sqrt{I} \\ |y - \sqrt{S}x_k| > \sqrt{I} \end{array} \right\} \text{The IC receiver decodes } x_\ell \text{ if } d_{y,\ell} < d_{y,k} \text{ (i.e. } y \text{ is closer to } x_\ell\text{);} \\ \text{Case 2: } \left. \begin{array}{l} |y - \sqrt{S}x_\ell| > \sqrt{I} \\ |y - \sqrt{S}x_k| \leq \sqrt{I} \end{array} \right\} \text{The IC receiver decodes } x_\ell \text{ if } d_{y,\ell} + d_{y,k} < 2\sqrt{I}; \\ \text{Case 3: } \left. \begin{array}{l} |y - \sqrt{S}x_\ell| \leq \sqrt{I} \\ |y - \sqrt{S}x_k| > \sqrt{I} \end{array} \right\} \text{The IC receiver decodes } x_\ell \text{ if } d_{y,\ell} + d_{y,k} \geq 2\sqrt{I}; \\ \text{Case 4: } \left. \begin{array}{l} |y - \sqrt{S}x_\ell| \leq \sqrt{I} \\ |y - \sqrt{S}x_k| \leq \sqrt{I} \end{array} \right\} \text{The IC receiver decodes } x_\ell \text{ if } d_{y,\ell} \geq d_{y,k} \text{ (i.e. } y \text{ is further from } x_\ell\text{);} \end{array}$$

where $d_{y,\ell} = |y - \sqrt{S}x_\ell|$ is the Euclidean distance between y and x_ℓ . In other words, each decoding region depends not only on the minimum distance but also the maximum distance and the middle two cases that cause “sliced areas” as seen in Table I. Hence, the IC decoder produces decoding regions that spread across multiple regions rather than being concentrated around constellation point as in the AWGN case.

TABLE I: THE OPTIMAL AND SUBOPTIMAL IC DECODING REGIMES FOR 8-PSK AT $S_{dB} = 10$ IN DIFFERENT REGIMES.

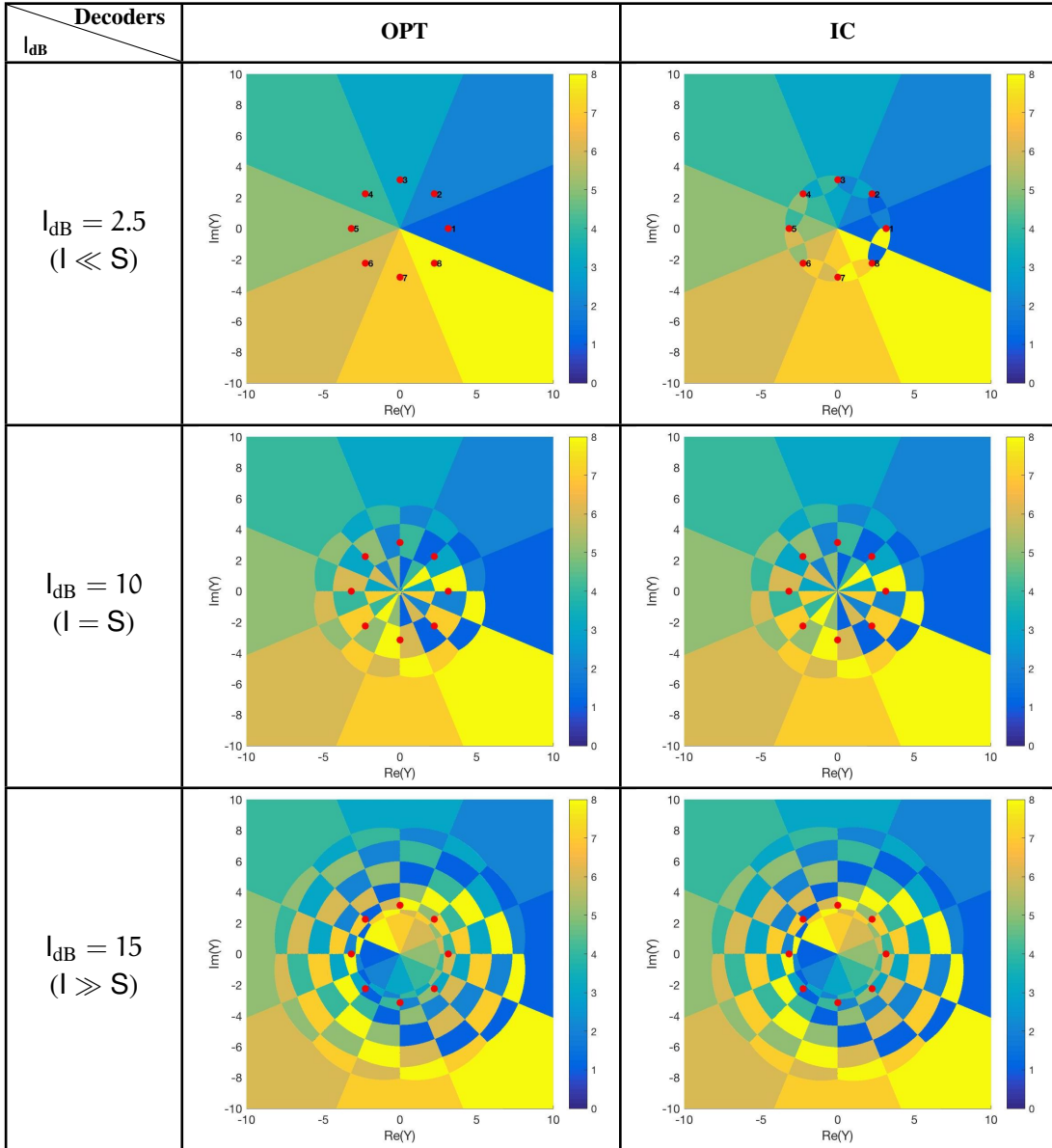


Table I shows the optimal and suboptimal decoding regions for an 8-PSK constellation at $S_{\text{dB}} = 10$ dB in the low, mid, and high INR regimes. The red bullets represent the coordinates of the transmitted symbols $\{x_1, \dots, x_8\}$, and are numbered 1 to 8 with 1 on the positive real axis and the others having an increasing number going counterclockwise. The decoding regions of the suboptimal TIN decoder (not reported due to limited space) depends only on the minimum Euclidean distance and are the same as the optimal decoding regions at $I_{\text{dB}} = 0.25$ in Table I for all range of INR values. For the AWGN ($I = 0$) case, all decoders yield exactly the same decoding regions, based on the minimum distance only. At low INR ($I_{\text{dB}} = 0.25S_{\text{dB}}$), we see that the decoding regions of the IC decoder shows visual differences compared with those of the optimal decoder. At mid INR ($I_{\text{dB}} = S_{\text{dB}}$), the IC decoder produces similar shapes (but slightly larger) as the optimal decoder. At high INR ($I_{\text{dB}} = 1.5S_{\text{dB}}$), the suboptimal IC decoding regions are almost identical as the optimal ML decoding regions.

Based on these results, we expect the TIN decoder to be very good at low INR ($I \ll S$); as I increases, the optimal decoding regions start to spread to nearby regions and the IC decoder should be better than the TIN decoder at mid INR ($I \cong S$); as I further increases much higher than S , the IC decoder should be very good and actually approach the performance of the optimal one at high INR ($I \gg S$). This intuition will be formalized next.

2.4 Symbol Error Rate (SER) Analysis

We analyze the SER at low and high INR using suboptimal TIN decoder in Equation 2.3 and IC decoder in Equation 2.4.

Low INR regime: The probability of error of the optimal receiver is upper bounded by that of the TIN receiver and is given by

$$\begin{aligned}
P_e^{(\text{OPT})} &\leq P_e^{(\text{TIN})} = \frac{1}{M} \sum_{\ell=1}^M \mathbb{P} \left[|Y - \sqrt{S}x_\ell|^2 > \min_{k:k \neq \ell} |Y - \sqrt{S}x_k|^2 \mid X = x_\ell \right] \\
&= \frac{1}{M} \sum_{\ell=1}^M \mathbb{P} \left[Z_{\text{eq}} > \min_{k:k \neq \ell} \left(\frac{\sqrt{S}|x_k - x_\ell|}{2} - \sqrt{I} \cos(\Theta) \right) \right] \\
&= \frac{1}{M} \sum_{\ell=1}^M \mathbb{E}_\Theta \left[Q \left(\sqrt{\frac{Sd_{\min}^2}{2}} - \sqrt{2I} \cos(\Theta) \right) \right], \tag{2.7}
\end{aligned}$$

where $d_{\min} = \min_{k:k \neq \ell} |x_k - x_\ell|$ is the minimum Euclidean distance between symbols. We can see that the SER of the TIN decoder depends only on the cardinality and the minimum distance of the constellation. Notice that the expression in Equation 2.7 without the extra term $\sqrt{2I} \cos(\Theta)$ is in fact the SER of an ML decoder for the AWGN-only channel.

High INR regime: Recall the expression for Y_{eq} in Equation 2.5, the probability of error of the optimal receiver is upper bounded by that of the IC receiver and is given by

$$\begin{aligned}
P_e^{(\text{OPT})} &\leq P_e^{(\text{IC})} = \frac{1}{M} \sum_{\ell=1}^M \mathbb{P} \left[|Y_{\text{eq}} - \sqrt{S}r_\ell|^2 > \min_{k:k \neq \ell} |Y_{\text{eq}} - \sqrt{S}r_k|^2 \mid X = x_\ell \right] \\
&\stackrel{I \gg S \gg 1}{\approx} \frac{1}{M} \sum_{\ell=1}^M \mathbb{P} \left[Z_{\text{eq}} \text{sign}(r_k - r_\ell) > \min_{k:k \neq \ell} \frac{\sqrt{S}|r_k - r_\ell|}{2} \right] \\
&\approx \frac{1}{M} \sum_{\ell=1}^M \mathbb{E}_\Theta \left[Q(\Delta_{k,\ell}^+(\Theta)) + Q(\Delta_{k,\ell}^-(\Theta)) \right], \tag{2.8}
\end{aligned}$$

where

$$r_\ell = \Re\{e^{-j\Theta} x_\ell\} \text{ for } \ell \in [1 : M], \tag{2.9}$$

$$\Delta_{k,\ell}^+(\Theta) = \min_{k \neq \ell: \text{sign}(r_k - r_\ell) > 0} \sqrt{\frac{S}{2}} |r_k - r_\ell|, \tag{2.10}$$

$$\Delta_{k,\ell}^-(\Theta) = \min_{k \neq \ell: \text{sign}(r_k - r_\ell) < 0} \sqrt{\frac{S}{2}} |r_k - r_\ell|. \quad (2.11)$$

We note that the approximation in Equation 2.8 does not have a simple interpretation as Equation 2.7 in terms of geometric properties of the constellation; it is, however, easy to evaluate numerically.

Next we analyze the SER expressions in Equation 2.7 and Equation 2.8 for the following commonly-used constellations, and evaluate its performance based on the Nearest Neighbor Union Bound (NNUB).

2.4.1 Pulse-Amplitude Modulation (PAM)

Low INR regime: For $l < S$, the probability of error of the TIN decoder in Equation 2.7 is

$$P_{e,\text{PAM}}^{(\text{ML})} \leq P_{e,\text{PAM}}^{(\text{TIN})} \approx 2 \left(1 - \frac{1}{M}\right) \mathbb{E}_\Theta \left[Q \left(\sqrt{\frac{6S}{M^2 - 1}} - \sqrt{2l} \cos(\Theta) \right) \right] \text{ by NNUB,}$$

where the term $2 \left(1 - \frac{1}{M}\right)$ indicates the number of nearest neighbors for a PAM as in the AWGN case.

High INR regime: For $l \gg S$, the probability of error of the IC decoder in Equation 2.8 is

$$P_{e,\text{PAM}}^{(\text{ML})} \leq P_{e,\text{PAM}}^{(\text{IC})} \stackrel{l \gg S \gg 1}{\approx} 2 \left(1 - \frac{1}{M}\right) \mathbb{E}_\Theta \left[Q \left(\sqrt{\frac{6S}{M^2 - 1}} \cos^2(\Theta) \right) \right] \text{ by NNUB.}$$

2.4.2 Square Quadrature Amplitude Modulation (Square-QAM)

Low INR regime: For $l < S$, the probability of error of the TIN decoder in Equation 2.7 is

$$P_{e,\text{QAM}}^{(\text{map})} \leq P_{e,\text{QAM}}^{(\text{TIN})} \approx 4 \left(1 - \frac{1}{\sqrt{M}}\right) \mathbb{E}_\Theta \left[Q \left(\sqrt{\frac{3S}{M - 1}} - \sqrt{2l} \cos(\Theta) \right) \right] \text{ by NNUB,}$$

where the term $4\left(1 - \frac{1}{\sqrt{M}}\right)$ indicates the number of nearest neighbors for a square-QAM as in the AWGN case. Detailed derivation as well as the exact SER and union bound expressions of the TIN decoder for the square M -QAM can be found in Appendix C.

High INR regime: For $I \gg S$, the probability of error of the IC decoder is given by Equation 2.8 as it does not seem possible to express the functions $\Delta_{k,\ell}^{\pm}(\Theta)$, in Equation 2.10 and Equation 2.11, in simple terms for the square M -QAM but they can be simply evaluated numerically.

2.4.3 Phase-Shift Keying (PSK)

Low INR regime: For $I < S$, the probability of error of the TIN decoder in Equation 2.7 is

$$P_{e,\text{PSK}}^{(\text{ML})} \leq P_{e,\text{PSK}}^{(\text{TIN})} \approx 2 \mathbb{E}_{\Theta} \left[Q \left(\sqrt{2S} \sin \left(\frac{\pi}{M} \right) - \sqrt{2I} \cos(\Theta) \right) \right] \text{ by NNUB,}$$

where 2 indicates the number of nearest neighbors for a PSK as in the AWGN case. Detailed derivation as well as the exact SER and union bound expressions of the TIN decoder for the M -PSK can be found in Appendix D.

High INR regime: For $I \gg S$, the error probability of the IC decoder in (Equation 2.8) is

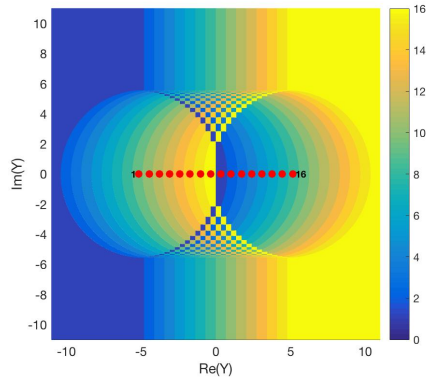
$$P_{e,\text{PSK}}^{(\text{ML})} \leq P_{e,\text{PSK}}^{(\text{IC})} = P_{e,\text{PSK}|x_M}^{(\text{IC})} \stackrel{I \gg S \gg 1}{\approx} \mathbb{P} \left[\text{sign}(r_M - r_\ell) \left(Z_{\text{eq}} + \frac{\sqrt{S}}{2} (r_M - r_\ell) \right) < 0, \exists \ell < M \right], \quad (2.12)$$

where $r_M - r_\ell = 2 \sin \left(\frac{\phi_\ell}{2} \right) \sin \left(\frac{\phi_\ell}{2} - \Theta \right)$, $\phi_\ell = \frac{2\pi\ell}{M}$, and r_ℓ is defined in Equation 2.9. Further simplifications of the probability in Equation 2.12 do not seem possible but this can be numerically evaluated.

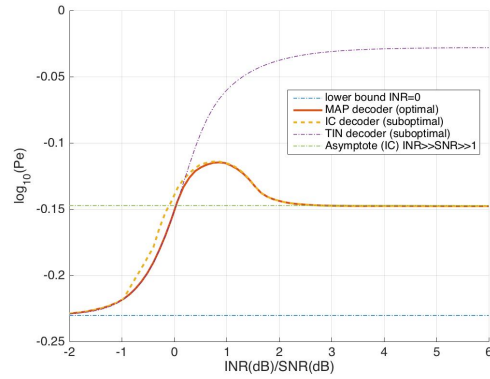
With these SER approximations for the above classical constellations, we can then investigate the performance of various decoders in terms of error rates.

2.5 SER Performance Evaluations

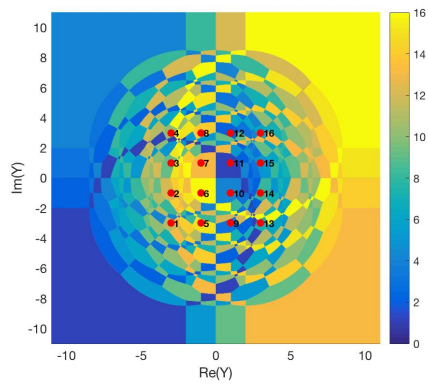
Here we report the optimal decoding regions and SER performance for the practically-used 16-PAM, 16-QAM, and 16-PSK constellations. The optimal decoding regions at $S = 10$ dB and $I = 15$ dB are shown on the left hand side of Fig. Figure 1, and the red bullets denote the locations of the transmitted symbols $\{x_1, \dots, x_{16}\}$ numbered from 1 to 16. The SER curves are plotted against the INR (in dB) normalized by a fixed SNR of 10 dB on the right hand side of Fig. Figure 1. The lowest SER is always at $I = 0$ corresponding to the AWGN-only channel case. The SER increases with INR until it reaches its highest value, which takes place around for $I_{\text{dB}}/S_{\text{dB}} \approx 1$, then it decreases and flattens out to the asymptote given by the SER expression for the IC decoder at $I \rightarrow \infty$. Recall that at high INR, the communications receiver can estimate and cancel the radar interference, thus, the SER starts to decrease around $I \approx S$. However, part of the communications signal is also removed, which reduces the effective SNR at the receiver. Hence, the SER does not reduce all the way to the lower SER bound for the interference-free case as the channel at high INR becomes the real-valued phase-fading Gaussian channel. Note that at low INR the TIN decoder provides an excellent approximation for the performance of the optimal ML decoder, while the IC decoder does not perform as well in this regime. The opposite holds at high INR. In general, the IC decoder is actually not much off compared to the optimal ML decoder, even at low INR.



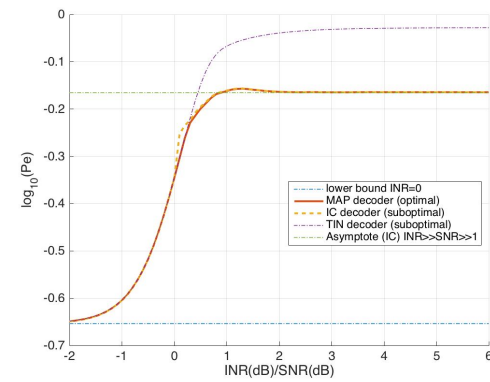
(a) Optimal decoding regions 16-PAM.



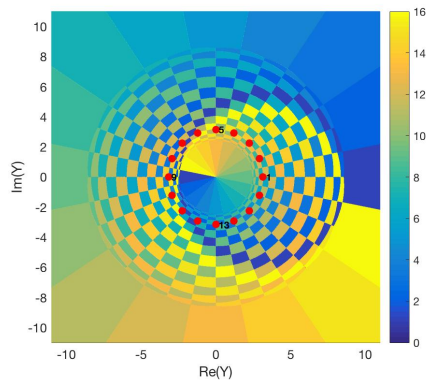
(b) SER for 16-PAM.



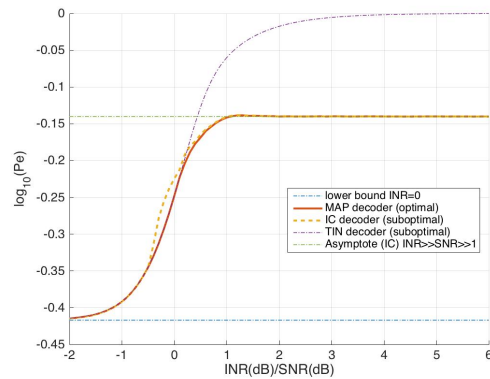
(c) Optimal decoding regions 16-QAM.



(d) SER for 16-QAM.



(e) Optimal decoding regions 16-PSK.



(f) SER for 16-PSK.

Figure 1: Decoding regions for $S = 10$ dB and $I = 15$ dB, and SER for $S = 10$ dB vs. I in dB.

2.6 Signal Constellation Design

Given the performance of commonly-used constellations designed for the AWGN-only channel, a natural question is whether constellations optimized for the channel in Equation 2.2 have different shapes and properties. Here we are interested in designing a two-dimensional signal constellation so as to optimize the communications system performance in the presence of a radar signal. We look at two optimization problems under predetermined conditions: one is to maximize the transmission rates, and the other is to minimize the error rates. The performance comparison of the designed constellations and the practically-used ones is later presented.

2.6.1 Optimization Formulation for Maximizing the Transmission Rates

Our goal is to design a signal constellation with the largest rate (number of points M) subject to given average SER and average power constraints. Mathematically, for some desired maximum SER value of ε , we aim to determine

$$M^{(\text{OPT})}(\varepsilon) = \max M \quad (\text{Equation 2.13})$$

$$\text{s.t. } P_e(\mathcal{X}) \leq \varepsilon, \quad (2.13\text{a})$$

$$\mathcal{X} = \{x_1, \dots, x_M\}, \quad (2.13\text{b})$$

$$\frac{1}{M} \sum_{\ell=1}^M |x_\ell|^2 \leq 1, \quad x_\ell \in \mathbb{C}, \quad (2.13\text{c})$$

where $P_e(\mathcal{X})$ denotes the SER approximations of the optimal ML decoder for the constellation \mathcal{X} , and is given by Equation 2.7 and Equation 2.8 in the low and high INR regimes, respectively. This implies that the location of the signal constellation points in Equation 2.13b has to be optimized to satisfy the

constraints for the average SER in Equation 2.13a and average power in Equation 2.13c. Note that such a constellation needs not necessarily exist as the SER has to be at least as large as that of a binary-PAM.

In our optimization algorithm, we start by fixing the number of points M (as small as 2) and find such a signal constellation that minimizes the SER approximations of the optimal decoder; if the SER for the found constellation satisfies Equation 2.13a then we increase M by 1 and repeat these steps until the maximum SER requirement is violated. We then obtain the constellation \mathcal{X} with the largest number of points $M^{(\text{OPT})}$ under the given constraints.

2.6.2 Optimization Formulation for Minimizing the Error Rates

The dual problem of the constellation design that minimizes the SER subject to a fixed transmission rate (constellation size) and an average power constraint is considered here and is given by

$$P_e^{(\text{OPT})}(M) = \min P_e(\mathcal{X}) \quad (\text{Equation 2.14})$$

$$\text{s.t. } \mathcal{X} = \{x_1, \dots, x_M\}, \quad (2.14a)$$

$$\frac{1}{M} \sum_{\ell=1}^M |x_\ell|^2 \leq 1, \quad x_\ell \in \mathbb{C}. \quad (2.14b)$$

In our optimization algorithm, we fix the constellation of size M and find such a signal constellation that minimizes the SER approximations of the optimal decoder within a given power budget.

In both (non-convex) optimization problems, we use the numerical Global Search (GS) method in [51], as implemented in the MATLAB Global Optimization Toolbox. Global Search is a gradient-based algorithm that uses a scatter-search mechanism to generate multiple randomized start points then analyzes and rejects the points that are not likely to improve the best local minimum found so far. Global

Search aims to find the function's global minima; it attempts this by finding and comparing different local minima of smooth nonlinear optimization problem. Thus, the results are not always guaranteed to be globally optimal. In order to minimize the chance of having found a local optimum, we run the GS method multiple times with different starting points as well as other optimization parameters.

2.6.3 Optimization Results for Constellations with Maximal Rates

We show here the results from the optimization problem in Subsection 2.6.1, in which we aim to design a two-dimensional signal constellation that can achieve the largest number of points M subject to average power and error rate constraints.

Table II reports the designed constellations with maximum number of points M for fixed ϵ of 10^{-3} , 10^{-5} , and 10^{-6} at $S_{\text{dB}} = 10, 15$ and 20 and $I_{\text{dB}} = 0.25S_{\text{dB}}$. We observe that a triangle is initially formed with just 3 points then more points are added to form more triangles next to one another. At $\epsilon = 10^{-6}$ and $S_{\text{dB}} = 20$, the designed constellation of $M = 7$ points looks like a hexagon with a center point. As we relax the SER requirements to allow for more transmitted points, we observe that the designed constellations are shaped as concentric hexagons with multiple layers; for example, only 8 points are allowed for transmission under a given SER constraint of $\epsilon = 10^{-5}$ while 12 points can be sent for $\epsilon = 10^{-3}$. Generally, the shape of the designed constellation tends to a hexagonal lattice (the best packing in two dimensions) as the number of points increases.

Table III reports the designed constellations with maximum number of points M for fixed ϵ of $10^{-0.82}$, $10^{-1.15}$, and $10^{-1.48}$ at $S_{\text{dB}} = 10, 20$ and 30 and $I = 2S_{\text{dB}}$. Notice that the error rate constraints are set relatively high; this is due to the low SNR range in our optimization examples (see Appendix E for more details). We observe that the designed constellations are shaped as unequally-spaced PAM. The

TABLE II: DESIGNED CONSTELLATIONS WITH MAXIMUM TRANSMISSION RATES AT VARIOUS S_{dB} AND $I_{dB} = 0.25S_{dB}$.

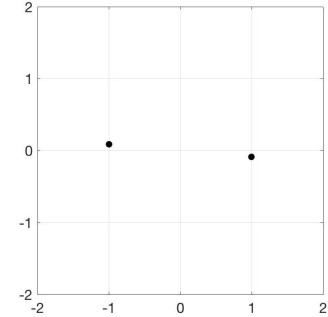
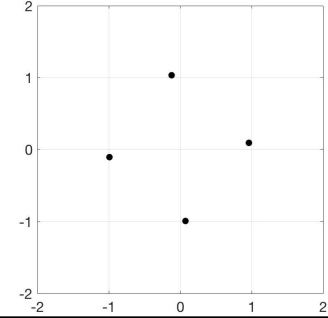
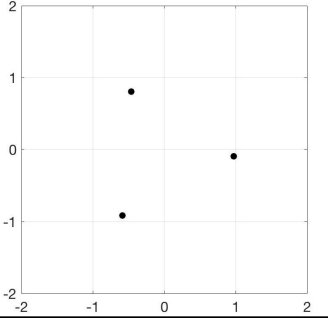
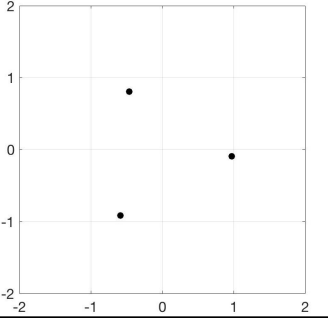
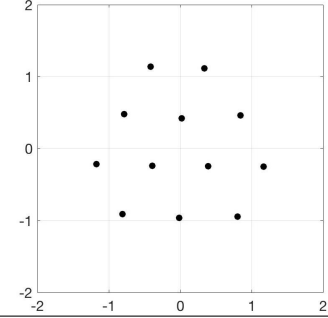
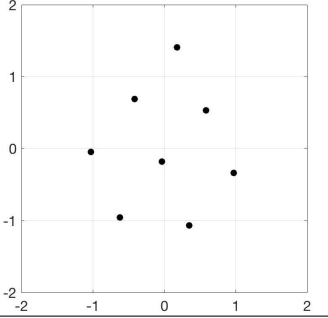
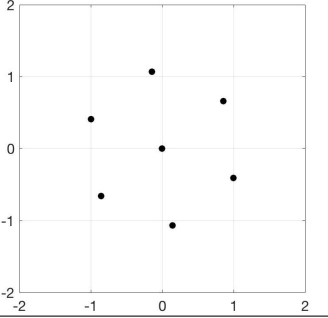
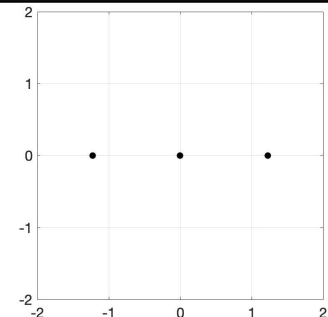
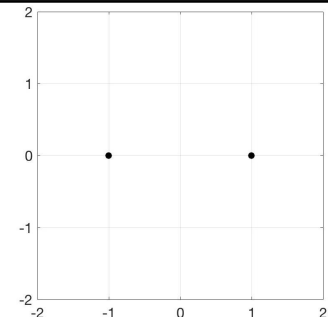
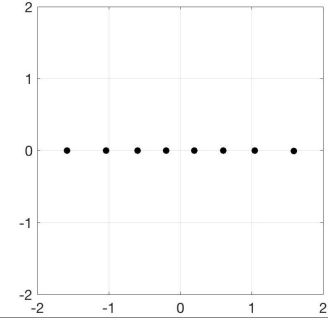
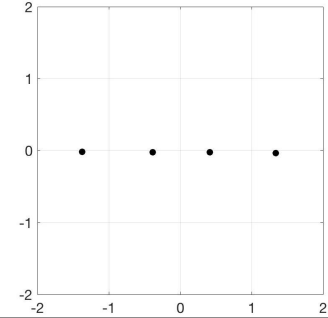
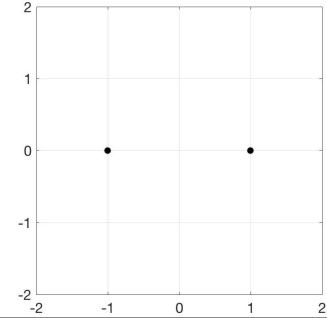
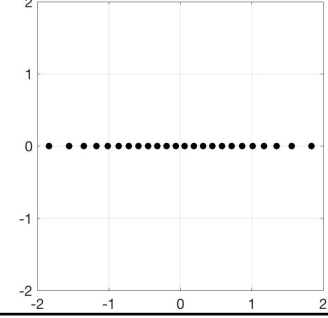
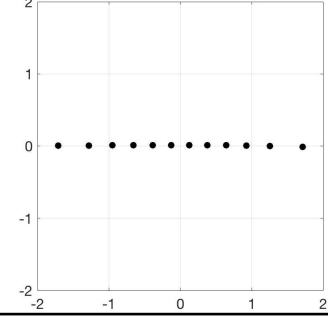
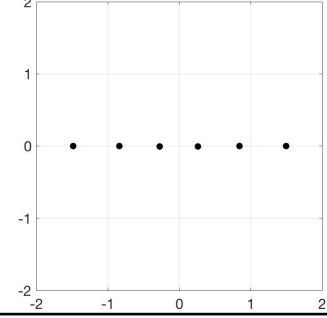
$S_{dB} \backslash \epsilon$	10^{-3}	10^{-5}	10^{-6}
10		No constellations satisfying the fixed SER of 10^{-5} at $S = 10$ dB are found.	No constellations satisfying the fixed SER of 10^{-6} at $S = 10$ dB are found.
15			
20			

TABLE III: DESIGNED CONSTELLATIONS WITH MAXIMUM TRANSMISSION RATES AT VARIOUS S_{dB} AND $I_{dB} = 2S_{dB}$.

$S_{dB} \backslash \epsilon$	$10^{-0.82}$	$10^{-1.15}$	$10^{-1.48}$
10			<p>No constellations satisfying the fixed SER of $10^{-1.48}$ at $S = 10$ dB are found.</p>
20			
30			

intuition is that the constellation points are placed as far apart from one another as possible (given the average power constraint) so as to result in larger possible minimum distances. Recall that the channel is equivalent to a real-valued phase-fading channel in the high INR regime so it makes intuitive sense that the points are placed according to the optimal packing in one dimension (at least at high SNR), which is the equi-lattice (equally-spaced points on a straight line).

2.6.4 Optimization Results for Constellations with Minimum Error Rates

We show here the results from the optimization problem in Subsection 2.6.2, in which we aim to design a two-dimensional signal constellation that can yield the lowest SER subject to average power and fixed constellation size constraints.

Table IV reports the designed constellations with minimum symbol error rates for fixed number of points M of 4, 8, and 16 at $S_{\text{dB}} = 20$ and $I_{\text{dB}} = 0.25S_{\text{dB}}$ for the TIN decoder and $I_{\text{dB}} = 2S_{\text{dB}}$ for the IC decoder as well as at $I \cong S$ for the optimal decoder in Equation 2.2. We observe that the designed constellation tends to shape like a concentric hexagon when $I \ll S$, while it tends to shape like a PAM but with unequally-spacing between symbols when $I \gg S$. Notice that the shapes of the designed constellations for minimizing the error rates are the same as those of the complimentary problem of maximizing the transmission rates. We heuristically observe that the highest SER takes place in the range of INRs close to SNR. We expect to see a transitioning between a hexagonal-like constellation at low INR and a PAM-like one at high INR around $I \cong S$. However, depending on the SNR, modulation scheme and constellation size, the exact point of $\frac{I_{\text{dB}}}{S_{\text{dB}}}$ in which the transitioning occurs is unpredictable. Therefore, an exhaustive search for the INRs is required to properly design a constellation. In this constellation design in the intermediate regime, we look at $S_{\text{dB}} = 20$ and $I_{\text{dB}} = 20, 25, \text{ and } 28$ for

TABLE IV: DESIGNED CONSTELLATIONS WITH MINIMUM SER AT $S_{dB} = 20$ AND $I_{dB} \cong 0.25S_{dB}, S_{dB}$ AND $2S_{dB}$ for $M = 4, 8,$ AND 16 .

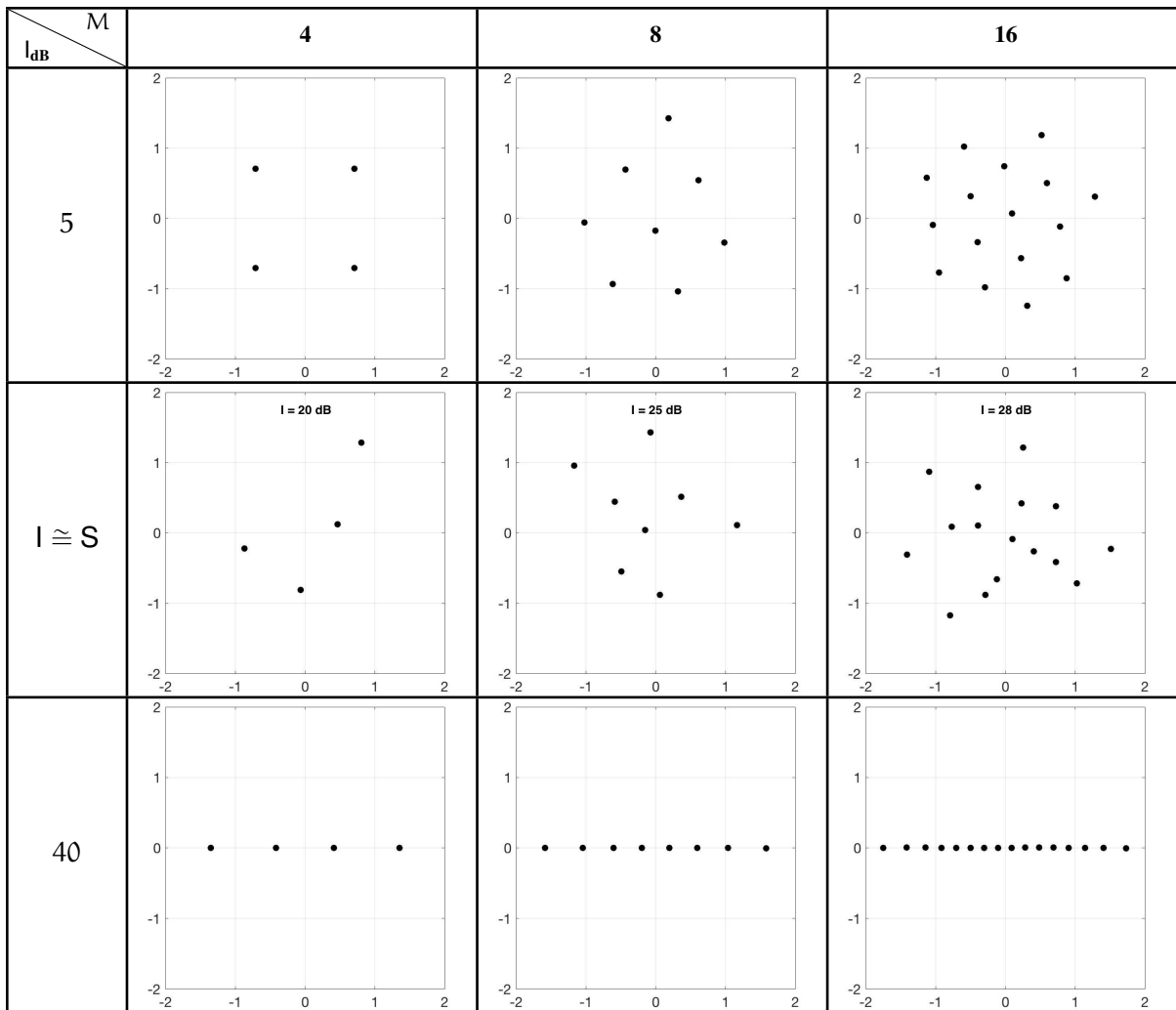


TABLE V: COMPARISON OF MAXIMUM M FOR DIFFERENT CONSTELLATIONS FOR $\varepsilon = 10^{-1}$.

(a) TIN Decoder at various S_{dB} and $I_{dB} = 0.25S_{dB}$.

S_{dB} \ Constellation	10	15	20
PAM	$M = 3, P_e = 10^{-1.2210}$	$M = 5, P_e = 10^{-1.0241}$	$M = 7, P_e = 10^{-1.3020}$
PSK	$M = 4, P_e = 10^{-1.3706}$	$M = 8, P_e = 10^{-1.0835}$	$M = 13, P_e = 10^{-1.1219}$
OPT	$M = 4, P_e = 10^{-1.3725}$	$M = 11, P_e = 10^{-1.0301}$	$M = 26, P_e = 10^{-1.0562}$

(b) IC Decoder at various S_{dB} and $I_{dB} = 2S_{dB}$.

S_{dB} \ Constellation	10	20	30
PAM	$M = 2, P_e = 10^{-1.2377}$	$M = 5, P_e = 10^{-1.0838}$	$M = 15, P_e = 10^{-1.0290}$
PSK	$M = 2, P_e = 10^{-1.2377}$	$M = 5, P_e = 10^{-1.0020}$	$M = 11, P_e = 10^{-1.0001}$
OPT	$M = 2, P_e = 10^{-1.2377}$	$M = 5, P_e = 10^{-1.0882}$	$M = 16, P_e = 10^{-1.0192}$

$M = 4, 8,$ and $16,$ respectively. We observe that the hexagon stretches into the straight line in the mid INR regime.

2.6.5 Performance Comparison

Here we compare the performance, in terms of transmission rates and error rates, of the designed constellations with the classical ones. Numerical results show that our designed constellations outperform the others.

Table V compares the largest rate M of the designed constellations with the practical ones, which are PAM and PSK in our examples, subject to the SER upper bounded by $\varepsilon = 10^{-1}$ at $S_{dB} = 10, 15,$ and 20 for low INR, and $S_{dB} = 10, 20,$ and 30 for high INR. At low INR ($I_{dB} = 0.25S_{dB}$), the designed constellations achieve the largest rates compared to PSK and PAM. As the radar interference increases, less points can be sent. At high INR ($I_{dB} = 2S_{dB}$), the transmission rates achieved by PSK and PAM are

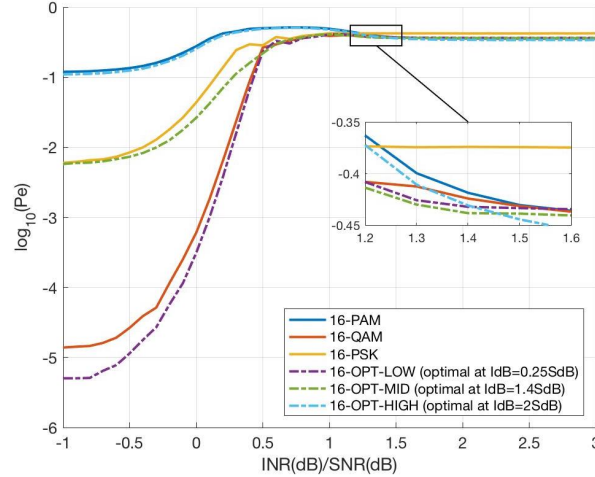


Figure 2: SER Comparison for $M = 16$ and $S = 20$ dB.

very competitive with the optimally designed constellations. In these cases, the designed constellations have advantages of yielding lower error rates than the classical ones.

Figure 2 shows the SER curves as a function of INR for the designed constellations with $M = 16$ points at $S_{dB} = 20$ in Table IV. Note that those constellations were optimized for a fixed INR and thus may not be optimal for the whole INR range. For comparison, we report the SER for the 16-PAM, 16-QAM, and 16-PSK, as representatives of the practical constellations. For low INR, the classical 16-PAM, 16-QAM, and 16-PSK are markedly suboptimal; the best performance is attained by the constellation 16-OPT-LOW, which was optimized for $l_{dB} = 0.25S_{dB} = 5$. For mid INR, the constellation 16-OPT-MID, which was optimized for $l_{dB} = 1.4S_{dB} = 28$, where the SER curve of the 16-OPT-LOW crosses that of the 16-OPT-HIGH, performs the best. For high INR, the classical 16-PAM is very competitive with the constellation 16-OPT-HIGH, which was optimized for $l_{dB} = 2S_{dB} = 40$.

At all range of INR, we remark the designed constellations outperform practically-used ones in terms of SER. Thus, one should send a hexagonal-like constellation in the weak radar interference regime, while a PAM constellation should be used in the very strong radar interference regime.

2.7 Conclusion

In this paper, we investigated a single-carrier system under the effect of a radar interference. We studied the error rate performance of uncoded complex-valued modulation schemes at a communications receiver in a complex-valued Gaussian channel with additive constant-amplitude and random-phase radar-induced interference. We derived the SER expressions for arbitrary constellations. The analysis of the error rate showed that the communications receiver should treat the radar interference of weak power as noise, while the receiver should estimate the radar interference of very strong power and cancel it. For small INR, the channel behaves as complex-valued AWGN channel. For large INR, the SER exhibits an irreducible “error floor” for large INR, which can be exactly characterized and behaves like narrowband fading channel with multiplicative fading that is perfectly known at the receiver but not at the transmitter. This unfortunately results in a loss of one of the complex dimensions as part of communications signal is lost in the interference cancellation process, which has been shown to be unavoidable in [40].

When considering actual wireless fading channels, this seems to imply that the channel model of interest, from the point of view of the communications receiver, is that of a narrowband fading model where the effective fading is the product of two terms: one corresponding to the classical (say Rayleigh or Rice) fading for the SNR, and the other due to the radar interference cancellation.

We then considered the designs of a two-dimensional signal constellation able to better handle this particular radar interference from two perspectives: maximizing the transmission rates subject to average power and error rate constraint, and minimizing the error rates subject to a power constraint. We observed that the designed constellation tends to a concentric hexagon shape when the radar interference power is low compared to that of the communications signal, while it tends to an unequally-spaced PAM shape for the high radar interference power regime. Although the detection scheme for the radar interference of intermediate power cannot be expressed in a closed-form, the result showed that the designed constellation is shaped as a transition from a hexagonal-like shape at weak radar interference to a PAM-like shape at very strong radar interference.

CHAPTER 3

A MULTI-CARRIER COMMUNICATIONS SYSTEM SUFFERING FROM RADAR INTERFERENCE

(This chapter was previously published as “Communications System Performance and Design in the Presence of Radar Interference”, in *IEEE Transactions on Communications* [52], and “Let’s share CommRad: Co-existing communications and radar systems”, in *Proceedings of IEEE Radar Conference (RadarConf)* [41].)

Narrowband single carrier systems, such as those studied in Chapter 2, are no longer the PHY layer choice for high speed networks. LTE, WiFi and foreseeably 5G are OFDM-based. In this section, we consider a general OFDM-based multi-carrier communications systems of N subcarriers and L OFDM blocks with additive white Gaussian noise and radar interference, as opposed to a simplified model of a single-carrier communications system, where $N = L = 1$, in the previous chapter.

3.1 System Model

The OFDM-based communications system operates at a carrier frequency of f_C Hz with N subcarriers over a total bandwidth of B_C Hz. The transmitted communications signal consists of L OFDM symbols, each with a symbol duration of T_C seconds. The pulsed radar system of interest operates at a carrier frequency f_R Hz over a bandwidth of B_R Hz. The pulse repetition interval (PRI) of the radar pulse $w_R(t)$ is given by T_R and each pulse has a width of τ_R seconds. The radar signal is assumed to

arrive at the communications receiver T_d seconds after the arrival of the communications signal. This time delay T_d is unknown at the communications receiver and is assumed random.

The communications receiver is assumed to sample in synchrony with the transmitted symbols, with the sampling period of $T_S = 1/B_C$ seconds, at the time instants $t = dT_S$, $d \in \mathbb{N}_0$. The time delay in samples is defined as $N_d = \lfloor \frac{T_d}{T_S} \rfloor$, which is also random.

At the OFDM receiver, the discrete-time complex-valued baseband received signal is expressed as

$$\mathbf{Y} = \sqrt{\mathbf{S}}\mathbf{X} + \mathbf{I} + \mathbf{Z} \in \mathbb{C}^{N \times L}, \quad (3.1)$$

where

- $\mathbf{S} \in \mathbb{R}_+^{N \times N}$ is a diagonal matrix containing the average Signal-to-Noise Ratios (SNRs) of the communications signal for the corresponding subcarriers,
- $\mathbf{X} \in \mathbb{C}^{N \times L}$ is a matrix of the transmitted symbols drawn from the equally-likely complex-valued signal constellation $\mathcal{X} = \{x_1, \dots, x_M\}$ subject to the average power constraint $\frac{1}{M} \sum_{\ell=1}^M |x_\ell|^2 \leq 1$,
- $\mathbf{I} \in \mathbb{C}^{N \times L}$ is a matrix of the radar interference with rows corresponding to the subcarriers and columns corresponding to the OFDM blocks. This matrix is a function of the random variable N_d , which represents the time delay in samples (justification given later), and
- $\mathbf{Z} \in \mathbb{C}^{N \times L}$ characterizes the proper-complex Gaussian noise, whose components are independent standard normal random variables.

The random variables $(\mathbf{X}, N_d, \mathbf{Z})$ are mutually independent and \mathbf{S} is fixed and known at the receiver.

The interference matrix \mathbf{I} is obtained by passing the received radar signal through the OFDM receiver chain. The received radar signal at the OFDM communications receiver on the k^{th} subcarrier and m^{th} OFDM block of the matrix \mathbf{I} – after sampling, removing the cyclic prefix of length N_{CP} samples, and performing an N -point Discrete Fourier Transform (DFT) – is given by (see [49] for detailed derivation)

$$I_{k,m} = \text{DFT} \left(v_{R,m}[n] e^{j2\pi\Delta_f n T_S} \right) e^{j\psi_m}, \quad n \in [0 : N - 1], \quad (3.2)$$

where $v_{R,m}[n] = w_R((n + mN_C + N_{\text{CP}} - N_d) T_S)$, $n \in [0 : N - 1]$, is the sampled version of the passband radar signal $w_R(t)$ during the m^{th} OFDM block, $N_C = \lceil \frac{T_C}{T_S} \rceil$ is the OFDM symbol duration in samples, $N_R = \lceil \frac{T_R}{T_S} \rceil$ is the pulse repetition interval of the radar signal in samples, $\Delta_f = f_R - f_C$ is the difference between the frequencies of the two systems, and the radar phase at the m^{th} block is defined as

$$\psi_m = 2\pi T_S (\Delta_f (mN_C + N_{\text{CP}}) - f_R N_d). \quad (3.3)$$

Note that some OFDM blocks might not experience the radar interference as in practice radar signals generally consist of periodic pulses of large amplitude and small duty-cycle while the communications signals usually have lower power and 100% duty-cycle (i.e., $\tau_R \leq T_C \leq T_R$). Let \mathcal{I} denote the set of OFDM block indices during which radar pulses take place, i.e., $\mathcal{I} = \left\{ \left\lfloor \frac{T_d + nT_R}{T_C} \right\rfloor \mid n \in \left[0 : \left\lfloor \frac{LT_C - T_d}{T_R} \right\rfloor \right] \right\}$. Also define ε_m as a binary indicator that is 1 if $m \in \mathcal{I}$, and 0 otherwise.

For a rectangular radar pulse, the sampled version of it for the m^{th} block of length N is given by

$$v_{R,m}[n] = \begin{cases} \varepsilon_m A_R, & c_m \leq n \leq d_m - 1, \\ 0, & \text{else,} \end{cases} \quad n \in [0 : N - 1], \quad (3.4)$$

and its corresponding DFT is given by

$$V_{R,m}[k] = \text{DFT}(v_{R,m}[n]) = \begin{cases} \frac{\varepsilon_m A_R}{\sqrt{N}} (d_m - c_m), & k = 0, \\ \frac{\varepsilon_m A_R}{\sqrt{N}} \frac{\sin(\pi k (d_m - c_m)/N)}{\sin(\pi k/N)} e^{-j\pi (d_m + c_m - 1) \frac{k}{N}}, & k \in [1 : N - 1], \end{cases} \quad (3.5)$$

where c_m and d_m denote the start and end of the non-zero content of $v_{R,m}[n]$, and A_R is its amplitude.

For blocks with no radar interference (i.e., with $\varepsilon_m = 0$), $c_m = 0$ and $d_m = 1$. Otherwise,

$$c_m = \begin{cases} N_d - N_{CP}, & N_d > N_{CP}, \\ 0, & \text{else,} \end{cases} \quad (3.6)$$

$$d_m = \begin{cases} n_R - N_{CP}, & n_R > N_{CP}, \\ 0, & \text{else,} \end{cases} \quad (3.7)$$

where $n_R = \lfloor \frac{\tau_R + T_d}{T_S} \rfloor$ indicates the end of the radar pulse at the OFDM receiver.

By substituting Equation 3.5 in Equation 3.2 and assuming that $\Delta_f N T_S$ is an integer, we can simplify the k^{th} and m^{th} entry of the radar interference matrix \mathbf{I} in Equation 3.2 as

$$I_{k,m} = V_{R,m} [(k - \Delta_f N T_S)_N] e^{j\psi_m} = V_{R,m} [k_N] e^{j\psi_m}$$

$$= \begin{cases} \frac{\varepsilon_m A_R}{\sqrt{N}} (d_m - c_m) e^{j\psi_m}, & k_N = 0, \\ \frac{\varepsilon_m A_R}{\sqrt{N}} \frac{|\sin(\pi k_N (d_m - c_m)/N)|}{\sin(\pi k_N/N)} e^{j\psi'_{k,m}}, & \text{otherwise,} \end{cases} \quad (3.8)$$

$$= A_{k,m} e^{j\Theta_{k,m}}, \quad k \in [0 : N - 1], m \in [0 : L - 1], \quad (3.9)$$

where $(a)_N$ denotes a modulo N , ψ_m is defined in Equation 3.3, $k_N = (k - \Delta_f N T_S)_N$, and

$$\psi'_{k,m} = \psi_m + \pi\beta_{k,m} - \pi \frac{k_N}{N} (d_m + c_m - 1), \quad (3.10)$$

$$\beta_{k,m} = \begin{cases} 0, & 0 \leq \left(\frac{k_N (d_m - c_m)}{N} \right)_2 \leq 1, \\ 1, & \text{else.} \end{cases} \quad (3.11)$$

The results in [49] shows that the PMF based on Equation 3.8 still closely resembles the actual PMF based on Equation 3.2 when $\Delta_f N T_S$ is a non-integer. Hence, we remark that Equation 3.8 is a good approximation for any $\Delta_f N T_S \in \mathbb{R}_+$.

The simplified expression in Equation 3.8 asserts that for those OFDM symbols and subcarriers that experience the radar interference, the joint distribution of $(A_{k,m}, \Theta_{k,m})$ is dominated by a single amplitude for which the phase is essentially uniform. This general conclusion from [49] is not restricted to rectangular radar pulses. Although here we have restricted attention to a rectangular radar pulse for analytical simplicity, other waveforms lead to qualitatively similar joint (amplitude and phase) distributions seen at the OFDM receiver, and are expected to lead to similar overall conclusions since our model requires only statistical knowledge of the phase. With this in mind, the following radar parameters are assumed to be known (or can be reliably estimated) at the OFDM receiver in our model: the

radar pulse shape including the radar pulse width (τ_R) and the radar carrier frequency (f_R) are generally either public record or can be obtained from the corresponding entity (e.g., a weather radar station), and the dominant radar signal's amplitude can be estimated as explained in Section 2.

Notice that the amplitude and phase of the radar interference at the k^{th} subcarrier and m^{th} OFDM block, denoted as $A_{k,m}$ and $\Theta_{k,m}$ in Equation 3.9, respectively, are functions of N_d . Thus, the radar interference matrix \mathbf{I} from the channel model in Equation 3.1 can be expressed as a deterministic function of the random variable N_d .

We conclude this section with a couple of remarks.

The radar pulse can interfere with two OFDM blocks rather than only one block as assumed in the above derivation; in this case, the radar pulse will arrive towards the end of the m^{th} block and extend to the start of the $(m+1)^{\text{th}}$ block. Following [47] and references therein for ATC radars, we assume that the radar pulse width is smaller than the cyclic prefix interval, i.e., $\tau_R < T_{CP}$. Thus, the first part of the radar pulse affects the data part of the m^{th} block, which increases the chance that the receiver makes an error; its second part, however, corrupts only the cyclic prefix part of the $(m+1)^{\text{th}}$ block, which will not contribute to a higher error rate at the $(m+1)^{\text{th}}$ block as its data is not damaged. As a result, the time lag between the communications and radar signals at the receiver falls within the range of the start of the radar-interfered OFDM block and the end of that block. Hence, this time delay T_d is assumed uniform on $[0, T_C - \tau_R)$ or, equivalently, the sampled time delay $N_d \sim \mathcal{U}\{[0 : N_C - n_w]\}$, where $n_w = \lfloor \frac{\tau_R}{T_S} \rfloor$ is the sampled radar pulse width.

Finally, for the case of $N = L = 1$ with the assumption that the radar PRI equals the OFDM symbol span, i.e., $T_R = T_C$, the amplitude of the radar interference in Equation 3.9 is approximately deterministic and its phase $\Theta_{k,m} = f(N_d)$ is in fact $\Theta \sim \mathcal{U}[0, 2\pi]$, as discussed in Chapter 2.

3.2 Detection Schemes

Based on the channel model of an OFDM receiver suffering from radar interference in Equation 3.1, we can finally derive its corresponding detection schemes. The channel conditional distribution of the discrete-time complex-valued received signal in Equation 3.1 is given by

$$f_{\mathbf{Y}|\mathbf{X}, N_d}(\mathbf{y}|\mathbf{x}, n_d) = \frac{e^{-[\mathbf{y} - \sqrt{\mathbf{S}}\mathbf{x} - \mathbf{i}(n_d)]^* \Sigma^{-1} [\mathbf{y} - \sqrt{\mathbf{S}}\mathbf{x} - \mathbf{i}(n_d)]}}{|\pi \Sigma|}, \quad \mathbf{y} \in \mathbb{C}^{N_L \times 1}, \quad \mathbf{x} \in \mathbb{C}^{N_L \times 1}, \quad (3.12)$$

and the radar interference matrix $\mathbf{i}(n_d) \in \mathbb{C}^{N_L \times 1}$ is a function of the random variable N_d with entries from Equation 3.8. \mathbf{A}^* and $|\mathbf{A}|$ denote the Hermitian transpose and determinant of matrix \mathbf{A} , respectively, and $\Sigma = \mathbb{E}_{N_d} \left[(\mathbf{y} - \sqrt{\mathbf{S}}\mathbf{x} - \mathbf{i}(n_d)) (\mathbf{y} - \sqrt{\mathbf{S}}\mathbf{x} - \mathbf{i}(n_d))^* \right]$ is the covariance matrix.

For any OFDM block of duration T_C to experience the radar interference, the radar pulse of width τ_R can arrive at the OFDM receiver anytime, as early as the same time as an OFDM symbol, but the radar pulse has to end by the end of that OFDM symbol. Thus, the time lag between the communications and radar signals is assumed uniformly distributed on $[0, T_C - \tau_R)$ or, equivalently, the time delay in samples $N_d \sim \mathcal{U}\{[0 : N_C - n_w]\}$, where $n_w = \lfloor \frac{\tau_R}{T_S} \rfloor$ is the radar pulse width in samples. This unknown time delay causes the received signal to be correlated in both time (OFDM symbols) and frequency (subcarriers). The optimal ML detector decodes N subcarriers and L blocks altogether. The suboptimal ML detectors are categorized into three cases, based on the correlation of the received signal: when it

considers the correlation in time only (referred to as the suboptimal time-correlated decoder); when it considers the correlation in frequency only (referred to as the suboptimal frequency-correlated decoder); and when it considers the received signal as uncorrelated (referred to as the suboptimal uncorrelated decoder or, also known as, the symbol-by-symbol detector). Next, we derive the decoding schemes for these decoders that minimize the probability of error.

3.2.1 Optimal ML Decoder

Based on the channel conditional distribution in Equation 3.12, the optimal receiver chooses an estimate of the transmitted symbol $\mathbf{X} = \mathbf{x}_\ell \in \mathbb{C}^{NL \times 1}$ for the received signal $\mathbf{Y} = \mathbf{y} \in \mathbb{C}^{NL \times 1}$

$$\begin{aligned} \hat{\ell}^{(\text{OPT})}(\mathbf{y}) &= \arg \max_{\substack{\mathbf{x}_\ell \in \{\mathbf{x}_1, \mathbf{x}_2, \dots, \mathbf{x}_{M^{NL}}\} \\ \mathbf{x}_\ell = [x_1 \ x_2 \ \dots \ x_{NL}]^T}} \sum_{n_d=0}^{N_C - n_w} f_{\mathbf{Y}|\mathbf{X}, N_d}(\mathbf{y}|\mathbf{x}_\ell, n_d) \cdot \mathbb{P}[N_d = n_d] \\ &= \arg \max_{\substack{\mathbf{x}_\ell \in \{\mathbf{x}_1, \mathbf{x}_2, \dots, \mathbf{x}_{M^{NL}}\} \\ \mathbf{x}_\ell = [x_1 \ x_2 \ \dots \ x_{NL}]^T}} \frac{\sum_{n_d=0}^{N_C - n_w} e^{-\frac{1}{\sigma^2} \sum_{m=0}^{L-1} \sum_{k=0}^{N-1} |y_{k,m} - \sqrt{S_{k,m}} [x_\ell]_{k,m} - i_{k,m}(n_d)|^2}}{(N_C - n_w + 1) \cdot (\pi\sigma^2)^{NL}}, \end{aligned} \quad (3.13)$$

where $[x_\ell]_{k,m}$ is the k^{th} (subcarrier) and m^{th} (OFDM block) entry of matrix \mathbf{x}_ℓ

3.2.2 Suboptimal Time-Correlated Decoder

The suboptimal time-correlated decoder ignores the correlation in frequency of the received signal and thus considers only the time correlation. We shall refer to this detector as the ‘‘SUBTIME’’ decoder.

The SUBTIME receiver chooses an estimate of the transmitted symbol $\mathbf{X}' = \mathbf{x}'_\ell \in \mathbb{C}^{L \times 1}$ for the received signal $\mathbf{Y}' = \mathbf{y}' \in \mathbb{C}^{L \times 1}$ for all the blocks at the k^{th} subcarrier

$$\hat{\ell}_k^{(\text{SUBTIME})}(\mathbf{y}') = \arg \max_{\substack{\mathbf{x}'_\ell \in \{\mathbf{x}'_1, \mathbf{x}'_2, \dots, \mathbf{x}'_{M_L}\} \\ \mathbf{x}'_\ell = [x_1 \ x_2 \ \dots \ x_L]^T}} \frac{\sum_{n_d=0}^{N_C - n_w} e^{-\frac{1}{\sigma^2} \sum_{m=0}^{L-1} |y_{k,m} - \sqrt{S_{k,m}} [x_\ell]_{k,m} - i_{k,m}(n_d)|^2}}}{(N_C - n_w + 1) \cdot (\pi\sigma^2)^L}. \quad (3.14)$$

The decoded block of size L at each k^{th} subcarrier in Equation 3.14 are then put into a block of size NL , denoted as $\hat{\ell}^{(\text{SUBTIME})}(\mathbf{y}) \in \mathbb{C}^{NL \times 1}$, for the error rate analysis in Section 3.3, and is given by

$$\hat{\ell}^{(\text{SUBTIME})}(\mathbf{y}) = \left[\hat{\ell}_{k=0}^{(\text{SUBTIME})}(\mathbf{y}'|_{m=0}) \ \dots \ \hat{\ell}_{k=N-1}^{(\text{SUBTIME})}(\mathbf{y}'|_{m=0}) \ \dots \ \hat{\ell}_{k=N-1}^{(\text{SUBTIME})}(\mathbf{y}'|_{m=L-1}) \right]^T. \quad (3.15)$$

3.2.3 Suboptimal Frequency-Correlated Decoder

The suboptimal frequency-correlated decoder ignores the correlation in time of the received signal and thus considers only the frequency correlation. We shall refer to this detector as the ‘‘SUBFREQ’’ decoder. The SUBFREQ receiver chooses an estimate of the transmitted symbol $\mathbf{X}'' = \mathbf{x}''_\ell \in \mathbb{C}^{N \times 1}$ for the received signal $\mathbf{Y}'' = \mathbf{y}'' \in \mathbb{C}^{N \times 1}$ for all the subcarriers at the m^{th} OFDM block

$$\hat{\ell}_m^{(\text{SUBFREQ})}(\mathbf{y}'') = \arg \max_{\substack{\mathbf{x}''_\ell \in \{\mathbf{x}''_1, \mathbf{x}''_2, \dots, \mathbf{x}''_{M_N}\} \\ \mathbf{x}''_\ell = [x_1 \ x_2 \ \dots \ x_N]^T}} \frac{\sum_{n_d=0}^{N_C - n_w} e^{-\frac{1}{\sigma^2} \sum_{k=0}^{N-1} |y_{k,m} - \sqrt{S_{k,m}} [x_\ell]_{k,m} - i_{k,m}(n_d)|^2}}}{(N_C - n_w + 1) \cdot (\pi\sigma^2)^N}. \quad (3.16)$$

The decoded block of size N at each m^{th} block in Equation 3.16 are then put into a block of size NL , denoted as $\hat{\ell}^{(\text{SUBFREQ})}(\mathbf{y}) \in \mathbb{C}^{NL \times 1}$, for the error rate analysis in Section 3.3, and is given by

$$\hat{\ell}^{(\text{SUBFREQ})}(\mathbf{y}) = \left[\hat{\ell}_{m=0}^{(\text{SUBFREQ})}(\mathbf{y}'') \quad \hat{\ell}_{m=1}^{(\text{SUBFREQ})}(\mathbf{y}'') \quad \dots \quad \hat{\ell}_{m=L-1}^{(\text{SUBFREQ})}(\mathbf{y}'') \right]^T. \quad (3.17)$$

3.2.4 Suboptimal Uncorrelated Decoder

The suboptimal uncorrelated decoder ignores the correlation in both frequency and time of the received signal and is basically a symbol-by-symbol detector. We shall refer to this detector as the ‘‘SUBNONE’’ decoder. The SUBNONE receiver chooses an estimate of the transmitted symbol $X = x_\ell \in \mathbb{C}$ for the received signal $Y = \mathbf{y} \in \mathbb{C}$ at the k^{th} subcarrier and m^{th} block

$$\hat{\ell}_{k,m}^{(\text{SUBNONE})}(\mathbf{y}) = \arg \max_{x_\ell \in \{x_1, x_2, \dots, x_M\}} \frac{1}{N_C - n_w + 1} \cdot \frac{1}{\pi \sigma^2} \sum_{n_d=0}^{N_C - n_w} e^{-\frac{1}{\sigma^2} |y_{k,m} - \sqrt{S_{k,m}} x_\ell - i_{k,m}(n_d)|^2}. \quad (3.18)$$

The decoded symbol at each m^{th} block and k^{th} subcarrier in Equation 3.18 are then put into a block of size NL , denoted as $\hat{\ell}^{(\text{SUBNONE})}(\mathbf{y}) \in \mathbb{C}^{NL \times 1}$, for the error rate analysis in Section 3.3, and is given by

$$\hat{\ell}^{(\text{SUBNONE})}(\mathbf{y}) = \left[\hat{\ell}_{0,0}^{(\text{SUBNONE})}(\mathbf{y}) \quad \dots \quad \hat{\ell}_{N-1,0}^{(\text{SUBNONE})}(\mathbf{y}) \quad \dots \quad \hat{\ell}_{0,L-1}^{(\text{SUBNONE})}(\mathbf{y}) \quad \dots \quad \hat{\ell}_{N-1,L-1}^{(\text{SUBNONE})}(\mathbf{y}) \right]^T. \quad (3.19)$$

Since the optimal receiver decodes the whole block (of L symbols and N subcarriers) of the received signal, its computation time increases with the constellation size and numbers of subcarriers and symbols. The suboptimal receivers reduce the decoding time by disregarding some or all of the correla-

tions in the received signal. Hence, the computational complexity (in terms of decoding time) for each decoder is:

- $O(M^{NL} \times NL \times (N_C - n_w))$ for OPTIMAL decoder,
- $O(M^L \times NL \times (N_C - n_w))$ for SUBTIME decoder,
- $O(M^N \times NL \times (N_C - n_w))$ for SUBFREQ decoder, and
- $O(1 \times NL \times (N_C - n_w))$ for SUBNONE decoder.

3.3 Error Rate Analysis

We now study the performance of the receivers in terms of error rate. Here we look at two types of error rates: BLock Error Rate (BLER) and Symbol Error Rate (SER). The BLER looks at all the $\hat{\ell}(\mathbf{y})$ blocks, each of size NL for all the L OFDM blocks and N subcarriers, and calculates how many blocks contain one or more symbol errors over the total number of blocks N_B , while the SER looks at how many incorrect symbols occur on average in each $\hat{\ell}(\mathbf{y})$ block. Mathematically, the block error rate, given that $\mathbf{x}_\ell \in \mathbb{C}^{NL \times 1}$ is transmitted, can be expressed as

$$\begin{aligned}
 \text{BLER} &= \sum_{\ell=1}^{M^{NL}} \mathbb{P}[\mathbf{X} = \mathbf{x}_\ell] \cdot \mathbb{P}[\hat{\ell}(\mathbf{y}) \neq \mathbf{x}_\ell \mid \mathbf{X} = \mathbf{x}_\ell] \\
 &= \frac{1}{M^{NL}} \sum_{\ell=1}^{M^{NL}} \mathbb{P} \left[\mathbb{E}_{N_d} [f_{\mathbf{Y}|\mathbf{X}, N_d}(\mathbf{y}|\mathbf{x}_\ell, n_d)] < \max_{n:n \neq \ell} \mathbb{E}_{N_d} [f_{\mathbf{Y}|\mathbf{X}, N_d}(\mathbf{y}|\mathbf{x}_n, n_d)] \mid \mathbf{X} = \mathbf{x}_\ell \right] \\
 &= \frac{1}{M^{NL}} \sum_{\ell=1}^{M^{NL}} \mathbb{P} \left[\sum_{n_d=0}^{N_C - n_w} e^{-\frac{1}{\sigma^2} [y - \sqrt{S}x_\ell - i(n_d)]^* [y - \sqrt{S}x_\ell - i(n_d)]} \right. \\
 &\quad \left. < \max_{n:n \neq \ell} \sum_{n_d=0}^{N_C - n_w} e^{-\frac{1}{\sigma^2} [y - \sqrt{S}x_n - i(n_d)]^* [y - \sqrt{S}x_n - i(n_d)]} \right]. \tag{3.20}
 \end{aligned}$$

It does not seem possible to analytically express Equation 3.20 in a closed form. Therefore, we proceed to use Monte Carlo simulation to approximate the block error rate calculation as

$$\text{BLER} \cong \frac{1}{N_B} \sum_{b=1}^{N_B} \varepsilon_b, \quad (3.21)$$

where the block error indicator is defined as

$$\varepsilon_b = \begin{cases} 1, & \hat{\ell}(\mathbf{y}_b) \neq [\mathbf{x}_\ell]_b, \\ 0, & \hat{\ell}(\mathbf{y}_b) = [\mathbf{x}_\ell]_b, \end{cases} \quad \hat{\ell}(\mathbf{y}_b) \in \mathbb{C}^{NL \times 1},$$

and $[\mathbf{x}_\ell]_b \in \mathbb{C}^{NL \times 1}$ is the transmitted symbol \mathbf{x}_ℓ for the b^{th} block from a total number of N_B blocks.

Similarly, the corresponding symbol error rate for a transmitted symbol $x_\ell \in \mathbb{C}$ can be expressed as

$$\begin{aligned} \text{SER} &= \sum_{\ell=1}^M \mathbb{P}[X = x_\ell] \cdot \mathbb{P} \left[\mathbb{E}_{N_d} [f_{Y|X, N_d}(y|x_\ell, \mathbf{n}_d)] < \max_{n:n \neq \ell} \mathbb{E}_{N_d} [f_{Y|X, N_d}(y|x_n, \mathbf{n}_d)] | X = x_\ell \right] \\ &= \frac{1}{M} \sum_{\ell=1}^M \mathbb{P} \left[\sum_{n_d=0}^{N_C - n_w} e^{-\frac{1}{\sigma^2} |y - \sqrt{S} x_\ell - i(n_d)|^2} < \max_{n:n \neq \ell} \sum_{n_d=0}^{N_C - n_w} e^{-\frac{1}{\sigma^2} |y - \sqrt{S} x_n - i(n_d)|^2} | X = x_\ell \right] \\ &\cong \frac{1}{NL \times N_B} \sum_{b=1}^{N_B} \sum_{s=1}^{NL} \varepsilon_{b,s}, \end{aligned} \quad (3.22)$$

where the symbol error indicator is defined as

$$\varepsilon_{b,s} = \begin{cases} 1, & [\hat{\ell}(\mathbf{y}_b)]_s \neq [\mathbf{x}_\ell]_{b,s}, \\ 0, & [\hat{\ell}(\mathbf{y}_b)]_s = [\mathbf{x}_\ell]_{b,s}, \end{cases}$$

and $[\hat{\ell}(\mathbf{y}_b)]_s \in \mathbb{C}$ is the estimate of the transmitted symbol $[\mathbf{x}_\ell]_{b,s}$ for the s^{th} element of the b^{th} block.

The BLER in Equation 3.21 and SER in Equation 3.22 for each decoder can be obtained as follows:

- For the optimal ML decoder, substitute $\hat{\ell}(\mathbf{y}_b) = \hat{\ell}^{(\text{OPT})}(\mathbf{y})$ from Equation 3.13.
- For the suboptimal time-correlated decoder, substitute $\hat{\ell}(\mathbf{y}_b) = \hat{\ell}^{(\text{SUBTIME})}(\mathbf{y})$ from Equation 3.15.
- For the suboptimal frequency-correlated decoder, substitute $\hat{\ell}(\mathbf{y}_b) = \hat{\ell}^{(\text{SUBFREQ})}(\mathbf{y})$ from Equation 3.17.
- For the suboptimal symbol-by-symbol decoder, substitute $\hat{\ell}(\mathbf{y}_b) = \hat{\ell}^{(\text{SUBNONE})}(\mathbf{y})$ from Equation 3.19.

3.4 Error Rate Performances of the Decoders

Next we evaluate the error rate performances of the decoders. The OFDM system operates at a carrier frequency of $f_C = 2.84952$ GHz with a total bandwidth of $B_C = 960$ kHz. The cyclic prefix has a length of $N_{CP} = 16$. The selection of the available bandwidth is consistent with an LTE communications system. In practical OFDM systems, N is generally greater than 64 but for computational efficiency here we consider examples with much smaller values of N . The pulsed radar system transmits a rectangular pulse of amplitude $A_R = 2.5$ every $T_R = 83.33$ μs at a carrier frequency of $f_R = 2.85$ GHz.

Based on the optimal decoder in Equation 3.13 and suboptimal decoders in Equation 3.14, Equation 3.16, and Equation 3.18 with the rectangular radar interference in Equation 3.8, we conduct various evaluations with different values for the number of subcarriers N , number of OFDM blocks L , and radar pulse width in samples n_w . The modulation schemes considered in this example are Binary Phase-Shift Keying (BPSK), Pulse-Amplitude Modulation (PAM), and Quadrature Amplitude Modulation (QAM), which are the commonly-used constellations.

TABLE VI: ERROR RATE (IN LOG-SCALE) COMPARISON OF THE RECEIVERS AT VARIOUS NUMBER OF SUBCARRIERS N , NUMBER OF OFDM BLOCKS L , AND RADAR PULSE WIDTH IN SAMPLES n_w .

Decoders Parameters	OPTIMAL	SUBTIME	SUBFREQ	SUBNONE
$N = 2, L = 1$ $n_w = 2, \text{BPSK}$	$\log(\text{BLER}) = -2.343$ $\log(\text{SER}) = -2.644$	$\log(\text{BLER}) = -2.338$ $\log(\text{SER}) = -2.639$	$\log(\text{BLER}) = -2.343$ $\log(\text{SER}) = -2.644$	$\log(\text{BLER}) = -2.338$ $\log(\text{SER}) = -2.639$
$N = 2, L = 2$ $n_w = 1, \text{BPSK}$	$\log(\text{BLER}) = -4.444$ $\log(\text{SER}) = -5.046$	$\log(\text{BLER}) = -3.688$ $\log(\text{SER}) = -4.288$	$\log(\text{BLER}) = -3.638$ $\log(\text{SER}) = -4.237$	$\log(\text{BLER}) = -3.269$ $\log(\text{SER}) = -3.871$
$N = 2, L = 2$ $n_w = 2, \text{BPSK}$	$\log(\text{BLER}) = -3.221$ $\log(\text{SER}) = -3.656$	$\log(\text{BLER}) = -3.217$ $\log(\text{SER}) = -3.652$	$\log(\text{BLER}) = -2.035$ $\log(\text{SER}) = -2.630$	$\log(\text{BLER}) = -2.032$ $\log(\text{SER}) = -2.627$
$N = 2, L = 2$ $n_w = 2, 4\text{-QAM}$	$\log(\text{BLER}) = -1.673$ $\log(\text{SER}) = -2.075$	$\log(\text{BLER}) = -1.560$ $\log(\text{SER}) = -1.996$	$\log(\text{BLER}) = -1.243$ $\log(\text{SER}) = -1.755$	$\log(\text{BLER}) = -1.177$ $\log(\text{SER}) = -1.697$
$N = 2, L = 2$ $n_w = 2, 4\text{-PAM}$	$\log(\text{BLER}) = -0.800$ $\log(\text{SER}) = -1.302$	$\log(\text{BLER}) = -0.800$ $\log(\text{SER}) = -1.302$	$\log(\text{BLER}) = -0.751$ $\log(\text{SER}) = -1.258$	$\log(\text{BLER}) = -0.751$ $\log(\text{SER}) = -1.258$
$N = 2, L = 4$ $n_w = 2, \text{BPSK}$	$\log(\text{BLER}) = -4.523$ $\log(\text{SER}) = -5.347$	$\log(\text{BLER}) = -4.523$ $\log(\text{SER}) = -5.347$	$\log(\text{BLER}) = -1.747$ $\log(\text{SER}) = -2.630$	$\log(\text{BLER}) = -1.744$ $\log(\text{SER}) = -2.627$
$N = 4, L = 2$ $n_w = 2, \text{BPSK}$	$\log(\text{BLER}) = -2.608$ $\log(\text{SER}) = -3.214$	$\log(\text{BLER}) = -2.531$ $\log(\text{SER}) = -3.175$	$\log(\text{BLER}) = -1.751$ $\log(\text{SER}) = -2.634$	$\log(\text{BLER}) = -1.746$ $\log(\text{SER}) = -2.629$
$N = 4, L = 2$ $n_w = 4, \text{BPSK}$	$\log(\text{BLER}) = -2.122$ $\log(\text{SER}) = -2.726$	$\log(\text{BLER}) = -1.947$ $\log(\text{SER}) = -2.557$	$\log(\text{BLER}) = -1.375$ $\log(\text{SER}) = -2.210$	$\log(\text{BLER}) = -1.340$ $\log(\text{SER}) = -2.122$
$N = 4, L = 4$ $n_w = 2, \text{BPSK}$	$\log(\text{BLER}) = -3.604$ $\log(\text{SER}) = -4.285$	$\log(\text{BLER}) = -3.457$ $\log(\text{SER}) = -4.234$	$\log(\text{BLER}) = -1.492$ $\log(\text{SER}) = -2.640$	$\log(\text{BLER}) = -1.488$ $\log(\text{SER}) = -2.635$

Table VI shows the BLER and SER performances of all the decoders for $S = 10$ dB at each sub-carrier. Table Table VI shows the BLER and SER performances of all the decoders with $S = 10$ dB at each subcarrier. As expected, numerical results indicate that the OPTIMAL decoder always outperforms the suboptimal decoders in terms of error rates, both block and symbol, and that the SUBNONE decoder (symbol-by-symbol detector) generally performs the worst as it ignores all the correlations. The SUBTIME decoder is optimal when there is only 1 channel in the system (i.e., $N = 1$) as there is no correlation in frequency. Similarly, the SUBFREQ decoder becomes optimal when there is only 1 OFDM block (i.e., $L = 1$) as there is no correlation in time. Generally, the SUBFREQ decoder performs competitively with (but usually slightly better than) the SUBNONE decoder; however, it does not perform as well as the SUBTIME decoder. This indicates that accounting for time correlation (i.e., decoding several OFDM blocks at once at the expense of increased complexity) is critical for good performance. There is a trade off between the computation time and error rates when using suboptimal decoders. Depending on an application, if the time complexity is a major constraint (especially for large values of M , N , and L) then the SUBTIME decoder is an excellent compromise. Notice that both the BLERs and SERs increase with the constellation size for the same system configurations as seen in the case where M increases from 2 to 4 (i.e., the third to fifth rows in Table Table VI), in which BPSK yields the lowest error rates while 4-PAM gives the highest error rates. Notice also that an increase in the radar pulse width degrades the performance of the system as seen in the case where n_w increases from 2 to 4 (i.e., the seventh and eighth rows in Table Table VI).

We finally conclude that among all the suboptimal receivers, the SUBTIME receiver consistently yields the lowest error rates except for the case when $L = 1$ in which the SUBFREQ receiver outperforms the SUBTIME receiver (i.e., the first row in Table VI).

3.5 Conclusion

We first introduced a more simple model of a single-carrier communications system with radar interference in Chapter 2. Here, we discussed a more complicated but practically relevant model of a multi-carrier communications system. We modeled the additive pulsed radar interference after being processed by an OFDM receiver and analyzed several optimal (in terms of minimizing the probability of error) and suboptimal detection schemes. The unknown time lag between radar and communications signals, modeled as a random variable, causes the received communications signal to be correlated in both time and frequency. We categorized the suboptimal decoders, based on the correlation, into three types: the suboptimal time-correlated decoder considers the correlation in time only; the suboptimal frequency-correlated decoder considers the correlation in frequency only; while the suboptimal uncorrelated decoder, also known as the symbol-by-symbol detector, ignores the correlation in both time and frequency. Finally, we evaluated the error rate performances of the receivers with an interfering rectangular radar signal via simulations and the result showed that the suboptimal time-correlated receiver performs the best while the suboptimal symbol-by-symbol receiver performs the worst.

We believe that our findings will help in effectively co-designing, or at least offering a baseline for comparison when radar and communications systems share the same spectrum.

CHAPTER 4

A RADAR SYSTEM SUFFERING FROM COMMUNICATIONS INTERFERENCE

(Parts of this chapter were submitted as “On Optimal ROCs for a Radar System Interfered by a Communications System”, to *IEEE International Conference Communications (ICC)* [53].)

In order to efficiently co-design the coexisting radar and communications systems, a good understanding of how each system affects one another is essential. In Chapters 2 and 3, we investigated the performance degradation of the single-carrier and multi-carrier communications systems in the presence of radar interference. Here in this chapter, we explore the complimentary problem, how the communications interference affects the radar system under the shared spectrum.

4.1 System Model

Before discussing the model of a radar system with communications interference and its performance, we first present the interfering communications system model.

Communications System Model

At the communications receiver, the un-interfered (for simplicity in establishing the interference model at the radar receiver) discrete-time complex-valued received signal is

$$Y_c = g_c X_c + Z_c, \quad (4.1)$$

where $g_c \in \mathbb{C}$ is the communications channel gain, $X_c \in \mathcal{X}_c$ is the equally likely unit-energy complex-valued communications symbol from the constellation \mathcal{X}_c , and Z_c is the zero-mean unit-variance proper-complex additive white Gaussian noise.

In this work, motivated by capacity approaching adaptive schemes used in modern wireless systems, we assume that the communications transmitter chooses \mathcal{X}_c as a function of the instantaneous SNR $|g_c|^2$ as follows. The rate attainable by using a good channel code mapped onto a finite constellation can be approximated as $\log(1 + |g_c|^2/\kappa)$ where $\kappa := -\frac{\ln(5 \text{ BER})}{1.5}$ [48, Chapter 9, Eqn (9.7)] is a function of the desired Bit Error Rate (BER). In this work, we assume that the communications constellation is a square QAM of cardinality $|\mathcal{X}_c| = 4^{\lfloor \log_4(1 + |g_c|^2/\kappa) \rfloor}$, which is a random variable that takes values in $m \in \{1, 4, 16, 64, \dots\}$ with probability

$$\begin{aligned} q_m &:= \Pr[|\mathcal{X}_c| = m] = \Pr\left[4^{\lfloor \log_4\left(1 + \frac{|g_c|^2}{\kappa}\right) \rfloor} = m\right] \\ &= F_{|g_c|^2}(\kappa(4m - 1)) - F_{|g_c|^2}(\kappa(m - 1)), \end{aligned} \quad (4.2)$$

where $F_{|g_c|^2}(\cdot)$ is the CDF of $|g_c|^2$. For example, for Rayleigh fading we have $q_m = e^{-\frac{\kappa(m-1)}{2\sigma_g^2}} - e^{-\frac{\kappa(4m-1)}{2\sigma_g^2}}$, where $\sigma_g^2 := \mathbb{E}[|g_c|^2]$ is the average SNR at the communications receiver.

Radar System Model

At the radar receiver with communication interference the received signal is

$$Y_r = h_r X_r + h_c X_c + Z_r, \quad (4.3)$$

where $|h_r|^2 = S_r$ is the SNR of the radar signal, $X_r \in \mathcal{X}_r = \{0, 1\}$ is the indicator function representing absent or present target at a specific location, $|h_c|^2 = S_c$ is the SNR of the communications signal, $X_c \in \mathcal{X}_c$ as before, and Z_r is the zero-mean unit-variance proper-complex additive white Gaussian noise. The random variables (X_c, X_r, Z_c, Z_r) are assumed to be mutually independent. In this work, we assume that at the radar receiver h_r is known and fixed, while g_c is random and not instantaneously known. Regarding knowledge of \mathcal{X}_c and h_c at the radar receiver, we shall consider the following scenarios:

1. [Case 4.2.1] both h_c and \mathcal{X}_c are known and fixed, and
2. [Case 4.2.2] h_c is known and fixed but \mathcal{X}_c is not, where \mathcal{X}_c is chosen according to (Equation 4.2) because the communications transmitter adapts its transmission based on the channel gain to its communications receiver, and
3. [Case 4.2.3] both h_c and \mathcal{X}_c are unknown, where h_c is Rayleigh distributed and independent of all other random variables, and \mathcal{X}_c is chosen according to (Equation 4.2).

When the channel gains (h_r, h_c) are fixed (Cases 4.2.1 and 4.2.2), we have

$$f_{Y_r|X_r, X_c}(y|k, x) = \frac{1}{\pi} e^{-|y - h_r k - h_c x|^2}, \quad (4.4)$$

while when only h_r is fixed and $h_c \sim \mathcal{N}_{\mathbb{C}}(\mu_c = 0, \sigma_c^2)$ and is independent of everything else (Case 4.2.3), we have

$$f_{Y_r|X_r, X_c}(y|k, x) = \frac{1}{\pi(1 + \sigma_c^2|x|^2)} e^{-\frac{1}{(1 + \sigma_c^2|x|^2)}|y - h_r k - \mu_c x|^2}. \quad (4.5)$$

4.2 Hypothesis Testing

We consider here the performance of the radar receiver posed as a binary composite hypothesis test. As opposed to the simple hypothesis test, where the distributions for both hypotheses are completely known, the composite hypothesis test must accommodate the unknown parameters. We are interested in the *Bayesian approach*, which requires the prior knowledge of the distributions of the unknown parameters and models the unknown parameters as realizations of random variables [46]. Since it is assumed that the statistical characterization of the communications system is known at the radar receiver, it is reasonable to employ the Bayesian ALRT for the optimal Neyman-Pearson detector. The two hypothesis to be considered are $H_k = \{X_r = k\}$ for $k \in \{0, 1\}$ corresponding to radar target absent and target present, respectively.

4.2.1 Case 1: Known Communications Constellation and Channel Gain

We start with the scenario in Case 4.2.1 where the likelihood function in Equation 4.4 is used for a fixed channel gain pair (h_r, h_c) . Recall that the points in the constellation are chosen uniformly with PMF $p(x) = \frac{1}{m}, \forall x \in \mathcal{X}_c : |\mathcal{X}_c| = m$. The (shifted by the known quantity $+|h_r|^2$) ALRT is given by

$$\begin{aligned}
 \text{ALRT}(y) &= \ln \frac{\sum_{a \in \mathcal{X}_c} p(a) f_{Y_r|X_r, X_c}(y|1, a)}{\sum_{b \in \mathcal{X}_c} p(b) f_{Y_r|X_r, X_c}(y|0, b)} + |h_r|^2 \\
 &= \ln \frac{\sum_{a \in \mathcal{X}_c} \frac{1}{|\mathcal{X}_c|} e^{-|y-h_r-h_c a|^2}}{\sum_{b \in \mathcal{X}_c} \frac{1}{|\mathcal{X}_c|} e^{-|y-h_c b|^2}} + |h_r|^2 \\
 &= \ln \frac{e^{-|y-h_r|^2} \sum_{a \in \mathcal{X}_c} e^{-|h_c a|^2 + 2\Re\{(y-h_r)^* h_c a\}}}{e^{-|y|^2} \sum_{b \in \mathcal{X}_c} e^{-|h_c b|^2 + 2\Re\{y^* h_c b\}}} + |h_r|^2
 \end{aligned}$$

$$\begin{aligned}
&= \ln \frac{e^{-|h_r|^2 + 2\Re\{y^* h_r\}} \sum_{a \in \mathcal{X}_c} e^{-|h_c a|^2 + 2\Re\{(y-h_r)^* h_c a\}}}{\sum_{b \in \mathcal{X}_c} e^{-|h_c b|^2 + 2\Re\{y^* h_c b\}}} + |h_r|^2 \\
&= 2\Re\{y^* h_r\} + \ln \frac{\sum_{a \in \mathcal{X}_c} e^{-|h_c a|^2 + 2\Re\{(y-h_r)^* h_c a\}}}{\sum_{b \in \mathcal{X}_c} e^{-|h_c b|^2 + 2\Re\{y^* h_c b\}}}, \tag{4.6}
\end{aligned}$$

where $2\Re\{y^* h_r\}$ corresponds to the case of no communications interference.

For the ALRT detector, let the probability of False Alarm (FA) be $P_{\text{FA};\text{ALRT}}(t) := \Pr[\text{ALRT}(Y_r) > t | H_0]$, and the probability of Correct Detection (CD) be $P_{\text{CD};\text{ALRT}}(t) := \Pr[\text{ALRT}(Y_r) > t | H_1]$. The ROC curve for a FA constraint $\epsilon \in [0, 1]$ is obtained as

$$P_{\text{CD};\text{ALRT}}^*(\epsilon) := \max_{t \in \mathbb{R}: P_{\text{FA};\text{ALRT}}(t) \leq \epsilon} P_{\text{CD};\text{ALRT}}(t). \tag{4.7}$$

A suboptimal detector is the GLRT, which “ignores” the prior distribution on the unknown parameters and instead “estimates” them by maximum likelihood. The (shifted by the known quantity $+|h_r|^2$) GLRT is given by

$$\begin{aligned}
\text{GLRT}(y) &= \ln \frac{\max_{a \in \mathcal{X}_c} f_{Y_r | X_r, \mathcal{X}_c}(y | 1, a)}{\max_{b \in \mathcal{X}_c} f_{Y_r | X_r, \mathcal{X}_c}(y | 0, b)} + |h_r|^2 \\
&= 2\Re\{y^* h_r\} + \ln \frac{\max_{a \in \mathcal{X}_c} e^{-|h_c a|^2 + 2\Re\{(y-h_r)^* h_c a\}}}{\max_{b \in \mathcal{X}_c} e^{-|h_c b|^2 + 2\Re\{y^* h_c b\}}} \\
&= 2\Re\{y^* h_r\} + \max_{a \in \mathcal{X}_c} \left(2\Re\{(y-h_r)^* h_c a\} - |h_c a|^2 \right) - \max_{b \in \mathcal{X}_c} \left(2\Re\{y^* h_c b\} - |h_c b|^2 \right). \tag{4.8}
\end{aligned}$$

Let the probability of FA for the GLRT detector be $P_{\text{FA};\text{GLRT}}(t) := \Pr[\text{GLRT}(Y_r) > t | H_0]$, and the probability of CD be $P_{\text{CD};\text{GLRT}}(t) := \Pr[\text{GLRT}(Y_r) > t | H_1]$. The ROC curve for a FA constraint $\epsilon \in [0, 1]$ is obtained as

$$P_{\text{CD};\text{GLRT}}^*(\epsilon) := \max_{t \in \mathbb{R}: P_{\text{FA};\text{GLRT}}(t) \leq \epsilon} P_{\text{CD};\text{GLRT}}(t). \quad (4.9)$$

4.2.2 Case 2: Known Communications Channel Gain but Unknown Constellation

We now move to the scenario in Case 4.2.2 where the likelihood function in Equation 4.4 is used for a fixed channel gain pair (h_r, h_c) , and $p(x, m) = \frac{1}{m}, \forall x \in \mathcal{X}_c : |\mathcal{X}_c| = m$ and zero otherwise. The ALRT is given by

$$\begin{aligned} \text{ALRT}(y) &= \ln \frac{\sum_m \sum_{\substack{\mathbf{a} \in \mathcal{X}_c: \\ |\mathcal{X}_c|=m}} p(\mathbf{a}, m) f_{Y_r|X_r, X_c}(y|1, \mathbf{a})}{\sum_n \sum_{\substack{\mathbf{b} \in \mathcal{X}_c: \\ |\mathcal{X}_c|=n}} p(\mathbf{b}, n) f_{Y_r|X_r, X_c}(y|0, \mathbf{b})} + |h_r|^2 \\ &= 2\Re\{y^* h_r\} + \ln \frac{\sum_m \sum_{\substack{\mathbf{a} \in \mathcal{X}_c: \\ |\mathcal{X}_c|=m}} \frac{q_m}{m} e^{-|h_c \mathbf{a}|^2 + 2\Re\{(y-h_r)^* h_c \mathbf{a}\}}}{\sum_n \sum_{\substack{\mathbf{b} \in \mathcal{X}_c: \\ |\mathcal{X}_c|=n}} \frac{q_n}{n} e^{-|h_c \mathbf{b}|^2 + 2\Re\{y^* h_c \mathbf{b}\}}}. \end{aligned} \quad (4.10)$$

With Equation 4.10, we then compute the equivalent of Equation 4.7.

The GLRT is similarly given by

$$\text{GLRT}(y) = \ln \frac{\max_m \max_{\substack{\mathbf{a} \in \mathcal{X}_c: \\ |\mathcal{X}_c|=m}} f_{Y_r|X_r, X_c}(y|1, \mathbf{a})}{\max_n \max_{\substack{\mathbf{b} \in \mathcal{X}_c: \\ |\mathcal{X}_c|=n}} f_{Y_r|X_r, X_c}(y|0, \mathbf{b})} + |h_r|^2$$

$$= 2\Re\{y^*h_r\} + \max_m \max_{\substack{\mathbf{a} \in \mathcal{X}_c: \\ |\mathcal{X}_c|=m}} \left(2\Re\{(y-h_r)^*h_c\mathbf{a}\} - |h_c\mathbf{a}|^2 \right) - \max_n \max_{\substack{\mathbf{b} \in \mathcal{X}_c: \\ |\mathcal{X}_c|=n}} \left(2\Re\{y^*h_c\mathbf{b}\} - |h_c\mathbf{b}|^2 \right). \quad (4.11)$$

With Equation 4.11, we then compute the equivalent of Equation 4.9.

4.2.3 Case 3: Unknown Communications Constellation and Channel Gain

We now move to the scenario in Case 4.2.3 where we use $p(x, m, h) = \frac{1}{m}f_{h_c}(h)$, $\forall x \in \mathcal{X}_c : |\mathcal{X}_c| = m$, $h \in \mathbf{C}$ and zero otherwise. The ALRT is given by

$$\begin{aligned} \text{ALRT}(y) &= \ln \frac{\int dh_1 f_{h_c}(h_1) \sum_m \sum_{\substack{\mathbf{a} \in \mathcal{X}_c: \\ |\mathcal{X}_c|=m}} p(\mathbf{a}, m) f_{Y_r|X_r, X_c}(y|1, \mathbf{a})}{\int dh_2 f_{h_c}(h_2) \sum_{\substack{\mathbf{b} \in \mathcal{X}_c: \\ |\mathcal{X}_c|=n}} p(\mathbf{b}, n) f_{Y_r|X_r, X_c}(y|0, \mathbf{b})} + |h_r|^2 \\ &= 2\Re\{y^*h_r\} + \ln \frac{\int dh_1 f_{h_c}(h_1) \sum_m \sum_{\substack{\mathbf{a} \in \mathcal{X}_c: \\ |\mathcal{X}_c|=m}} \frac{q_m}{m} e^{-|h_1\mathbf{a}|^2 + 2\Re\{(y-h_r)^*h_1\mathbf{a}\}}}{\int dh_2 f_{h_c}(h_2) \sum_n \sum_{\substack{\mathbf{b} \in \mathcal{X}_c: \\ |\mathcal{X}_c|=n}} \frac{q_n}{n} e^{-|h_2\mathbf{b}|^2 + 2\Re\{y^*h_2\mathbf{b}\}}}. \end{aligned} \quad (4.12)$$

With Equation 4.12, we then compute the equivalent of Equation 4.7. Note that if the fading is Rayleigh then we can use Equation 4.5 with $\mu_c = 0$, which already has ‘‘averaged out’’ h_1 and h_2 , to get

$$\text{ALRT}(y) = |h_r|^2 + \ln \frac{\sum_m \sum_{\substack{\mathbf{a} \in \mathcal{X}_c: \\ |\mathcal{X}_c|=m}} \frac{q_m}{m} \frac{1}{\pi(1+\sigma_c^2|a|^2)} e^{-\frac{|y-h_r|^2}{1+\sigma_c^2|a|^2}}}{\sum_n \sum_{\substack{\mathbf{b} \in \mathcal{X}_c: \\ |\mathcal{X}_c|=n}} \frac{q_n}{n} \frac{1}{\pi(1+\sigma_c^2|b|^2)} e^{-\frac{|y|^2}{1+\sigma_c^2|b|^2}}}. \quad (4.13)$$

The GLRT is similarly given by

$$\begin{aligned}
\text{GLRT}(\mathbf{y}) &= \ln \frac{\max_{h_1} \max_m \max_{\substack{\mathbf{a} \in \mathcal{X}_c: \\ |\mathcal{X}_c|=m}} f_{Y_r|X_r, X_c}(\mathbf{y}|\mathbf{1}, \mathbf{a})}{\max_{h_2} \max_n \max_{\substack{\mathbf{b} \in \mathcal{X}_c: \\ |\mathcal{X}_c|=n}} f_{Y_r|X_r, X_c}(\mathbf{y}|\mathbf{0}, \mathbf{b})} + |\mathbf{h}_r|^2 \\
&= 2\Re\{\mathbf{y}^* \mathbf{h}_r\} + \ln \frac{\max_m \max_{\substack{\mathbf{a} \in \mathcal{X}_c: \\ |\mathcal{X}_c|=m}} e^{-|h_1^{\text{OPT}} \mathbf{a}|^2 + 2\Re\{(\mathbf{y} - \mathbf{h}_r)^* h_1^{\text{OPT}} \mathbf{a}\}}}{\max_n \max_{\substack{\mathbf{b} \in \mathcal{X}_c: \\ |\mathcal{X}_c|=n}} e^{-|h_2^{\text{OPT}} \mathbf{b}|^2 + 2\Re\{\mathbf{y}^* h_2^{\text{OPT}} \mathbf{b}\}}} \\
&\stackrel{(a)}{=} 2\Re\{\mathbf{y}^* \mathbf{h}_r\} + |\mathbf{y} - \mathbf{h}_r|^2 - |\mathbf{y}|^2 = |\mathbf{h}_r|^2, \tag{4.14}
\end{aligned}$$

where in (a) we used the optimal values $h_1^{\text{OPT}} = \frac{\mathbf{y} - \mathbf{h}_r}{a}$ and $h_2^{\text{OPT}} = \frac{\mathbf{y}}{b}$, or in other words, we have $\max f_{Y_r|X_r, X_c}(\mathbf{y}|\mathbf{k}, \mathbf{a}) = 1/\pi$. The fact that Equation 4.14 does not depend on the received value \mathbf{y} immediately raises a red flag regarding the suitability of GLRT as a surrogate of ARLT in this case – which was suggested for other scenarios in [45]. With Equation 4.14, we then compute the equivalent of Equation 4.9.

4.2.4 Unaltered radar receiver

Finally we use as a baseline performance in all the above cases the ROC of an “unaltered radar receiver,” that is, a radar that uses the same LRT as if there were only Gaussian noise; we have

$$\text{LRT}(\mathbf{y}) = 2\Re\{\mathbf{y}^* \mathbf{h}_r\}. \tag{4.15}$$

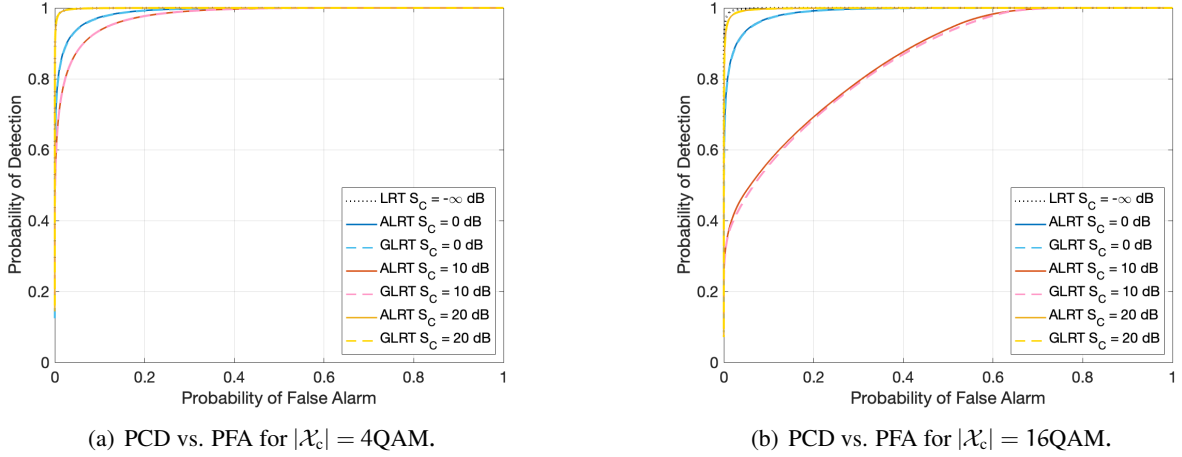


Figure 3: ROC for a fixed pair $(|h_r|^2, |h_c|^2) = (S_r, S_c)$ where $S_r = 10$ dB and $S_c = \{0, 10, 20\}$ dB.

We then compute the ROC curve for a FA constraint $\epsilon \in [0, 1]$ as

$$P_{\text{CD};\text{LRT}}^*(\epsilon) := \max_{t \in \mathbb{R}: P_{\text{FA};\text{LRT}}(t) \leq \epsilon} \Pr[2\Re\{Y_r^* h_r\} > t | H_1], \quad (4.16)$$

where the probability of false alarm for the LRT is defined as $P_{\text{FA};\text{LRT}}(t) := \Pr[2\Re\{Y_r^* h_r\} > t | H_0]$.

4.3 Receiver Operating Characteristic (ROC) Performance

In this section, the ROC curves for both the optimal ALRT and suboptimal GLRT detectors are numerically evaluated for the three scenarios presented in Section 4.2.

Composite Hypothesis Testing for Case 4.2.1

For a fixed channel gain pair $(|h_r|^2, |h_c|^2) = (S_r, S_c)$ and a known communications constellation \mathcal{X}_c at the radar receiver, we evaluate the ALRT and GLRT expressions in Equation 4.6 and Equation 4.8, respectively. Figure 3 shows the ROC curves for the ALRT (solid lines) and GLRT (dashed lines) at

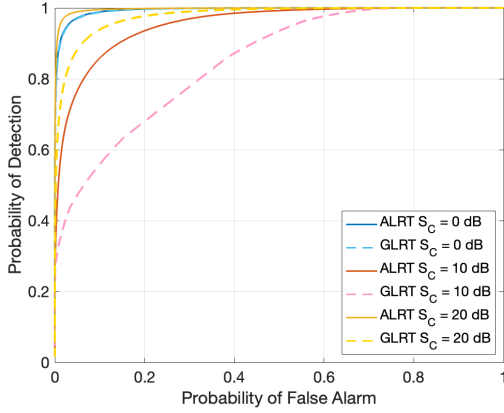
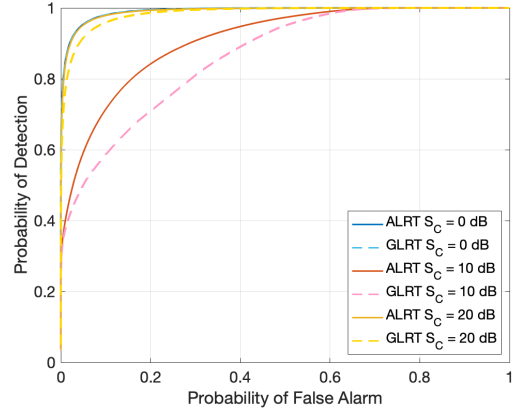
(a) PCD vs. PFA for $\mathbf{q} = [0.41, 0.52, 0.07]$.(b) PCD vs. PFA for $\mathbf{q} = [0.18, 0.41, 0.41]$.

Figure 4: ROC for a fixed pair $(|h_r|^2, |h_c|^2) = (S_r, S_c)$ where $S_r = 10$ dB and $S_c = \{0, 10, 20\}$ dB with $\mathcal{X}_c = \{\emptyset, 4\text{QAM}, 16\text{QAM}\}$.

$S_r = 10$ dB and $S_c \in \{0, 10, 20\}$ dB with $|\mathcal{X}_c| = 4\text{QAM}$ (see Figure 3(a)) or $|\mathcal{X}_c| = 16\text{QAM}$ (see Figure 3(b)). For comparison, the LRT detector ('dotted' line) in Equation 4.16, where the communications interference is absent, is plotted as an upper bound.

We observe that the detection performance for both the ALRT and GLRT detectors are hardly affected by the weak or strong communications interference, where the receiver can either ignore or successfully decode and cancel the interference, respectively. The worst performance occurs when the radar and communications signals have roughly equal powers, in which the GLRT visually shows slightly inferior performance to that of the ALRT as the communications constellation size increases.

Composite Hypothesis Testing for Case 4.2.2

For a fixed channel gain pair $(|h_r|^2, |h_c|^2) = (S_r, S_c)$ and an unknown \mathcal{X}_c that adapts to the communications channel gain $g_c \sim \mathcal{N}_{\mathbb{C}}(0, \sigma_g^2)$, we evaluate the ALRT and GLRT expressions in Equa-

tion 4.10 and Equation 4.11, respectively. Figure 4 shows the ROC curves for the ALRT and GLRT at $S_r = 10$ dB and $S_c \in \{0, 10, 20\}$ dB for $\sigma_g^2 \in \{10, 15\}$ dB. For a desired $\text{BER} = 10^{-3}$ and $\sigma_g^2 = 10$ dB we have $\mathbf{q} = [q_1, q_4, q_{16}] = [0.41, 0.52, 0.07]$ (see Figure 4(a)) while for $\sigma_g^2 = 15$ dB we have $\mathbf{q} = [0.18, 0.41, 0.41]$ (see Figure 4(b)) – where q_1 is the probability of the communications transmitter being silent, q_4 of using a 4QAM, q_{16} of using a 16QAM, while the remaining q_m are essentially zero to Matlab numerical precision.

We observe that the detection performance for the ALRT detector is hardly affected by the weak communications interference, while the strong interference slightly degrades the detection performance of the ALRT detector. As observed in Composite Hypothesis Testing for Case 4.2.1, the worst performance occurs when the radar and communications signals have roughly equal powers. Note that the ALRT performance is better with a smaller variance σ_g^2 due to the higher probability q_m of transmitting less points (small m), and that the GLRT can estimate the unknown communications parameters better with a higher power $\sigma_g^2 = \mathbb{E}[|g_c|^2]$. We also remark that the GLRT very well approximates the ALRT for weak interference and the GLRT performs quite worse for strong interference. However, the GLRT cannot capture the performance of the ALRT for comparable communications and radar powers.

Composite Hypothesis Testing for Case 4.2.3

Since $|h_r|^2 = S_r$ is fixed and known, but $h_c \sim \mathcal{N}_{\mathbb{C}}(0, \sigma_c^2)$ and \mathcal{X}_c are unknown, we evaluate the ALRT and GLRT expressions in Equation 4.12 and Equation 4.14, respectively. Figure 5 shows the ROC curves at $S_r = 10$ dB, $h_c \sim \mathcal{N}_{\mathbb{C}}(0, 10$ dB), for either $\sigma_g^2 = 10$ dB (see Figure 5(a)) or $\sigma_g^2 = 15$ dB (see Figure 5(b)), and $\text{BER} = 10^{-3}$.

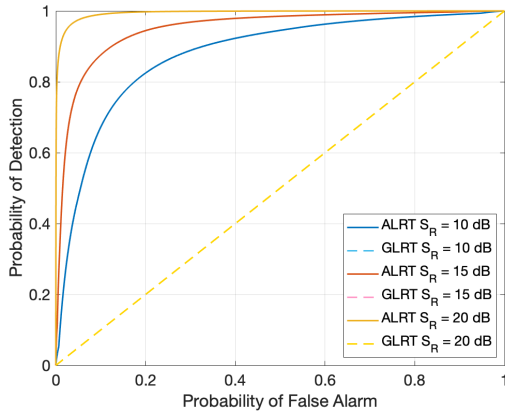
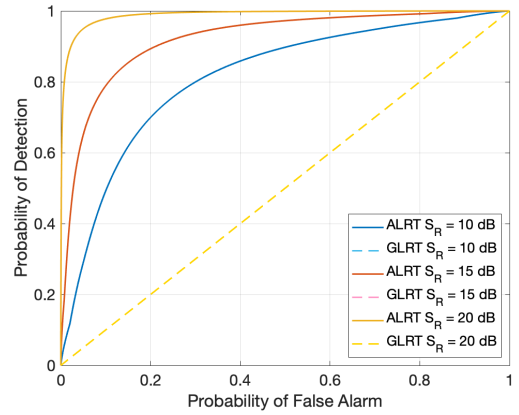
(a) PCD vs. PFA for $\mathbf{q} = [0.41, 0.52, 0.07]$.(b) PCD vs. PFA for $\mathbf{q} = [0.18, 0.41, 0.41]$.

Figure 5: ROC for a fixed $|h_r|^2 = S_r$ and a random $h_c \sim \mathcal{N}_C(0, 10 \text{ dB})$ with $|\mathcal{X}_c| = \{\emptyset, 4\text{QAM}, 16\text{QAM}\}$.

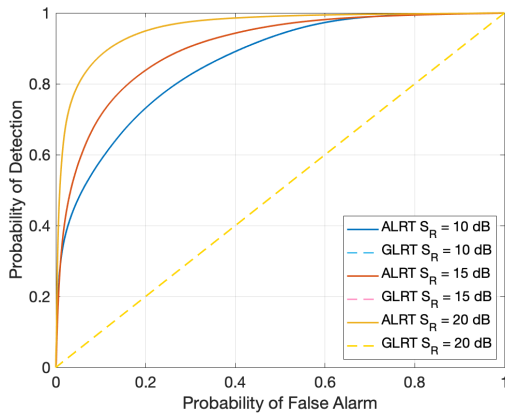
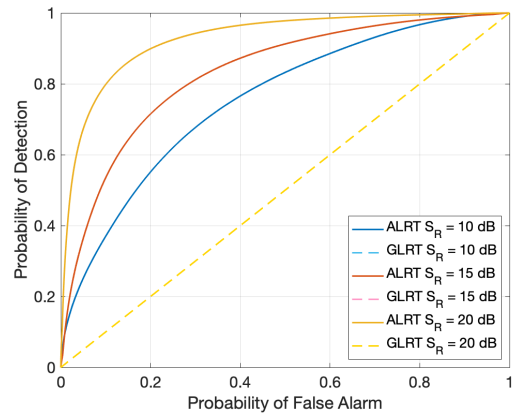
(a) PCD vs. PFA for $\mathbf{q} = [0.41, 0.52, 0.07]$.(b) PCD vs. PFA for $\mathbf{q} = [0.18, 0.41, 0.41]$.

Figure 6: ROC for a fixed $|h_r|^2 = S_r$ and a random $h_c \sim \mathcal{N}_C(0, 15 \text{ dB})$ with $|\mathcal{X}_c| = \{\emptyset, 4\text{QAM}, 16\text{QAM}\}$.

As expected, the detection performance increases with the radar power. As observed in Composite Hypothesis Testing for Case 2, the performance of the ALRT is better with a smaller variance σ_g^2 due to the higher chance of transmitting a symbol from a smaller communications size, i.e., less variability in \mathcal{X}_c . However, the performance of the GLRT does not change with different parameters (i.e, the dashed lines are all on top of one another). This is so because $\text{GLRT}(\mathbf{y})$ is a constant as seen in Equation 4.14; that is, the likelihood function for the received signal \mathbf{y} given hypothesis H_1 (target present) is the same as that given hypothesis H_0 (target absent), and thus the probabilities of CD and FA are the same for a specific threshold thereby yielding a straight line in the ROC curve. Thus, the GLRT detector should not be used in this scenario.

Note that the ROC curve for the ALRT at $S_r = 10$ dB in Figure 5, the ‘solid blue’ line, performs worse than those in Figure 4 due to the additional unknown parameter h_c in this scenario.

Similar to Figure 5 where the difference between the left and right figures is the distribution of g_c , Figure 6 plots the ROC curves for the ALRT and GLRT at $S_r = 10$ dB and $h_c \sim \mathcal{N}_C(0, 15 \text{ dB})$ for $|\mathcal{X}_c| = \{\emptyset, 4\text{QAM}, 16\text{QAM}\}$ with Rayleigh fading channel $g_c \sim \mathcal{N}_C(0, 10 \text{ dB})$ (see Figure 6(a)), and $g_c \sim \mathcal{N}_C(0, 15 \text{ dB})$ (see Figure 6(b)) to attain $\text{BER} = 10^{-3}$. Similar observations as for Figure 5 can be made here. For comparison, we remark that the ALRT performs better with a lower communications power range $\sigma_c^2 = \mathbb{E}[|h_c|^2]$, i.e. the ROC curves for the ALRT detector in Figure 5 are higher than those in Figure 6.

As opposed to the work in [45], which concluded that the GLRT detector generally well approximates the performance of the ALRT detector and could be used in place of the ALRT detector due to its computational efficiency, our simulated ROC performance suggests that this is not always the case.

When the radar receiver suffers from communications interference, we showed that the GLRT detector does not always perform closely to the optimal ALRT detector, especially when the communications constellation is chosen adaptively so as to satisfy an error rate constraint at the communications receiver and this is not known at the radar receiver. As a result, we conclude that the GLRT should not be used unless the interfering communications signal has relatively low or very high power compared to that of the radar signal, and that the implementation of the ALRT detector is strongly encouraged in the presence of communications interference.

4.4 Conclusion

In Chapter 2 and 3, we presented the error rate performance of a communications system in the presence of radar interference as well as a constellation design that is optimized for this particular system model. Here we analytically investigated the performance of the ALRT and GLRT detectors (based on the Bayesian approach and the maximum likelihood estimation, respectively) of a radar receiver in the presence of a communications signal for the following three scenarios: 1) the channel gains from both the communications transmitter and the radar transmitter to the radar receiver as well as the communications constellation are fixed and known; 2) the channel gains from both the communications transmitter and the radar transmitter to the radar receiver are fixed and known, but the communications constellation is not; and 3) only the channel gain from the radar transmitter to the radar receiver is known but the channel gain from the communications transmitter to the radar receiver and the communications constellation are not. In the latter two cases, the communications constellation is chosen adaptively at the communications transmitter from a set of square QAM constellations based on the channel gain to the communications receiver so as to satisfy the error rate constraint and this is not known at the radar

receiver. The receiver operating characteristic curves of the ALRT and GLRT detectors are examined where results showed that very strong communications interference hardly degrades the performance of the radar receiver as the receiver can successfully decode and cancel the interference, while intermediate communications interference of roughly the same power as the radar signal significantly affects the radar detection performance.

For the first scenario, we observed that the suboptimal GLRT detector very well approximates the optimal ALRT detector in spite of the power level of the communications interference; however, the GLRT shows slight performance degradation in the intermediate interference power regime as the communications constellation size grows. For the second scenario, we observed that the GLRT detector cannot capture the performance of the ALRT detector and thus should not be used in this intermediate interference regime, though the GLRT still effectively approximates the ALRT in both the weak and strong interference regimes. Interestingly, for the last scenario where the radar receiver has no knowledge of both the communications constellation size and the channel gain from the communications transmitter, the GLRT detector does not depend on the received signal and its ROC performance does not increase with the radar power. Thus, in this scenario, the GLRT should not be used at all despite its computational efficiency compared to the ALRT.

Note that as we have discussed so far the co-existing systems operate independently; however, one would eventually want to have a joint radar-communications detector that does both the average symbol error rate for the communications system and the receiver operating characteristic for the radar system.

CHAPTER 5

CONCLUSION

In this thesis, we have studied how co-existing communications and radar systems affect each other's performance as it is important to assess the performance of unaltered systems and understand what happens if the transmit sides of both systems are kept unaltered, which is the main focus of this work before embarking in a full co-design. These insights into the performance of unaltered systems can help guide future research directions in co-design synergies. We have investigated the performance limits of separate and unaltered co-existing and interfering communications and radar systems. The findings of this work are relevant for systems where changing the hardware may be too costly, but further digital signal processing of the baseband received signal is viable.

We started with the investigation of how an interfering radar signal degrades the performance of a single-carrier communications system under the shared spectrum, categorized by the strength of the radar interference with respect to the communications signal power. Then we extended our work to a two-dimensional communications constellation design with the goal of either maximizing the transmission rate subject to an average power and error rate constraints or minimizing the error rate under a power budget and a fixed transmission rate. Next, we explored the multi-carrier communications system performance suffering from radar interference, where the optimal and various suboptimal detectors are derived based on the correlation of the received signal at the OFDM receiver. Lastly, the performance of the radar receiver co-existing with the communications system was investigated, and the receiver

operating characteristic performance was numerically evaluated in Matlab and conclusions are finally drawn. The contributions of this thesis are summarized as follows:

- First, we looked at how the performance of a communications system degrades when co-exists with a radar system. We focused initially on a simpler single-carrier communications system. We approached the problem by modeling a single-carrier communications system with an interfering radar signal, where we considered a transmitter communicating with a receiver over a memory-less additive Gaussian noise and radar interference channel in Chapter 2. The radar interference is modeled as having a known constant amplitude and a known random phase uniformly distributed in $[0, 2\pi]$. We derived the Symbol Error Rate (SER) expressions of an uncoded communications system using using a complex-valued modulation scheme – specifically pulse amplitude modulation, quadrature amplitude modulation, and phase shift keying – at all range of radar signal power relative to the power of the communications signal. It has been shown that the radar interference of low power is treated as Noise while the communications receiver can subtract the strong radar interference along with part of the desired communications signal yielding an irreducible error floor. Based on the obtained SER expressions, we then optimized a communications constellation that maximizes the transmission rate, measured by the number of signal constellation points, subject to the average power and error rate not exceeding predetermined values as well as the ‘dual’ problem of the constellation design that minimizes the SER subject to a fixed rate since many widely-used complex-valued modulation schemes, such as QAM and PSK, are not necessarily optimal for this radar-interfered channel. We have shown that a constellation shaped as a concen-

tric hexagon is optimal in the weak interference regime while it transitions to an unequally-spaced straight line shaped constellation in the strong interference regime.

- Next, we considered a more complicated multi-carrier communications system affected by a radar interference. In Chapter 3, we assumed a general OFDM receiver with a radar signal arriving at an unknown time. We modeled the time delay between the two signals as uniformly distributed, which causes the received signal to be correlated in both time and frequency. Various decoders have been analyzed based on the correlation in the received signal. The optimal receiver considers the correlations in both time and frequency while suboptimal receivers consider only time or frequency or none of the above. The block and symbol error rate expressions were derived. Though no closed-form error rate expressions could be obtained, the performance of all decoders are evaluated via Monte Carlo simulation, where it has been shown that accounting for time correlation (i.e. decoding several OFDM blocks at once at the expense of increased complexity) is critical for good performance, and that the use of the suboptimal decoder that considers only the correlation in time of the received signal is recommended if the computation time is a major constraint since the computation time of the optimal decoder increases with the constellation size.
- Lastly, we studied the performance of a radar system with an interfering communications signal in Chapter 4. We derived two composite hypothesis testings: 1) the optimal Average Likelihood Ratio Test (ALRT) based on the Bayesian approach where the prior knowledge of the distributions of the unknown parameters is required, and 2) the suboptimal Generalized Likelihood Ratio Test (GLRT) which estimates the unknown parameters that maximize the likelihood. We considered scenarios based on the availability at the radar receiver of the communications constellation and

channel gain from the communications transmitter. Numerical results have shown that the GLRT detector efficiently captures the performance of the ALRT detector when both the channel gain and the communications constellation are both known; however, the performance of the GLRT detector degrades with less knowledge of the unknown parameters, and that the GLRT detector does not depend on the received signal or the power of the radar signal when the radar receiver has no knowledge of both the channel gain and the communications constellation.

These insights into the performance of separated and unaltered systems can help guide future research directions in co-design synergies. Eventually, one would want to have a joint radar-communications detector that can perform both the communications' average error rate and the radar's receiver operating characteristic.

CHAPTER 6

FUTURE DIRECTIONS

After the study of the interference impact on each system presented in the the previous chapters, the next logical step is to optimize the performance by jointly design the co-existing systems. We propose modeling the joint radar-communications system that can perform both communications error rate and radar target detection as a joint radar-communications receiver collocated with a radar transmitter, i.e., it is a joint radar transceiver combined with a communications receiver, paired with a communications transmitter located elsewhere. With this model, the statistical characterization of the radar and communications systems can be reasonably assumed known at the joint receiver, i.e. the channel gains from the communications and radar transmitters to the joint receiver as well as the communications constellation used are fixed and known at the joint receiver.

The discrete-time complex received signal at the joint radar-communications receiver is given by

$$Y = |h_r|X_r + h_cX_c + Z, \quad (6.1)$$

where $|h_r|^2 = S_r$ is the average Signal-to-Noise Ratio (SNR) of the radar signal, $X_r \in \mathcal{X}_r = \{0, 1\}$ is the indicator function representing absent or present target at a specific location $|h_c|^2 = S_c$ is the average SNR of the communications signal, $X_c \in \mathcal{X}_c$ is the equally likely unit-energy complex-valued communications symbol from the constellation \mathcal{X}_c , and Z is the zero-mean unit-variance proper-complex additive white Gaussian noise. Here we assume that the random variables (X_c, X_r, Z) are mutually independent

and that the channel gain pair (h_r, h_c) and communications constellation \mathcal{X}_c are fixed and known at the joint receiver.

With Equation 6.1, the likelihood function is given as

$$f_{Y|X_r, X_c}(y|a, b) = \frac{1}{\pi} e^{-|y - |h_r|a - h_c b|^2}. \quad (6.2)$$

There are many ways to approach this joint design problem, and here we propose the following directions.

6.1 Joint Bayesian Estimate

One solution is to jointly decode both the radar and communications signals together using the joint Bayesian estimate where the joint receiver chooses an estimate pair

$$\begin{aligned} (\hat{x}_r(y), \hat{x}_c(y)) &= \arg \max_{a \in \mathcal{X}_r, b \in \mathcal{X}_c} \Pr[X_r = a, X_c = b | Y = y] \cdot f_{Y|X_r, X_c}(y|a, b) \\ &= \arg \max_{a \in \mathcal{X}_r, b \in \mathcal{X}_c} \Pr[X_r = a | Y = y] \cdot \Pr[X_c = b | Y = y] \cdot \frac{1}{\pi} e^{-|y - |h_r|a - h_c b|^2}. \end{aligned} \quad (6.3)$$

This method is optimal in the sense of minimizing the joint error rate given by $\Pr[(\hat{x}_r(Y), \hat{x}_c(Y)) \neq (x_r, x_c) | Y = y]$.

6.2 Two-step Decoding Process

Another possible decoding method is a two-step decoding process, which aims to decode one signal of interest first then subtract its estimate off the received signal to remove the interference effect so

as to better estimate the other signal afterwards. Here we can investigate two methods: decode the communications signal first then radar, or decode the radar signal first then communications.

6.2.1 Communications First, Radar Next

For this method, the joint receiver will decode the communications symbol first where it chooses an estimate of the transmitted communications symbol $x_c \in \mathcal{X}_c$

$$\begin{aligned}\hat{x}_c(\mathbf{y}) &= \arg \max_{b \in \mathcal{X}_c} \Pr[X_c = b | Y = \mathbf{y}] \cdot \mathbb{E}_{X_r} [f_{Y|X_r, X_c}(\mathbf{y} | \mathbf{a}, b)] \\ &= \arg \max_{b \in \mathcal{X}_c} \frac{1-p}{\pi} e^{-|\mathbf{y}-h_c b|^2} + \frac{p}{\pi} e^{-|\mathbf{y}-|h_r|-h_c b|^2},\end{aligned}\quad (6.4)$$

where the error rate for the communications system can be calculated as $\Pr[\hat{x}_c(Y) \neq x_c | Y = \mathbf{y}]$.

Next, the communications symbol estimate is subtracted off the received signal where we have

$$Y' = Y - h_c \hat{x}_c(Y) = |h_r| \mathbf{a} + h_c (x_c - \hat{x}_c(Y)) + Z,$$

with a likelihood function $f_{Y'|X_r}(y' | \mathbf{a})$ that has no closed form and has to be calculated numerically. The

Likelihood Ratio Test (LRT) based on the residual received signal is expressed as

$$\text{LRT}'(y') = \ln \frac{f_{Y'|X_r}(y' | 1)}{f_{Y'|X_r}(y' | 0)}, \quad y' \in \mathbb{C}. \quad (6.5)$$

Then we can plot the ROC curve for the radar system as

$$P_{\text{CD}; \text{LRT}'}^*(\epsilon) := \max_{t \in \mathbb{R}: P_{\text{FA}; \text{LRT}'}(t) \leq \epsilon} P_{\text{CD}; \text{LRT}'}(t), \quad (6.6)$$

where the probabilities of correct detection and false alarms are given as $P_{\text{CD};\text{LRT}'}(t) := \Pr[\text{LRT}'(t) \geq t | X_r = 1]$ and $P_{\text{FA};\text{LRT}'}(t) := \Pr[\text{LRT}'(t) \geq t | X_r = 0]$, respectively.

6.2.2 Radar First, Communications Next

Similarly, the joint receiver will decode the radar symbol first where it chooses an estimate of the transmitted radar symbol $x_r \in \mathcal{X}_r$

$$\begin{aligned} \hat{x}_r(\mathbf{y}) &= \arg \max_{\mathbf{a} \in \mathcal{X}_r} \Pr[X_r = \mathbf{a} | Y = \mathbf{y}] \cdot \mathbb{E}_{X_c} [f_{Y|X_r, X_c}(\mathbf{y} | \mathbf{a}, \mathbf{b})] \\ &= \arg \max_{\mathbf{a} \in \mathcal{X}_r} \Pr[X_r = \mathbf{a} | Y = \mathbf{y}] \cdot \sum_{\mathbf{b} \in \mathcal{X}_c} \Pr[X_c = \mathbf{b}] \cdot \frac{1}{\pi} e^{-|\mathbf{y} - |\mathbf{h}_r| \mathbf{a} - \mathbf{h}_c \mathbf{b}|^2}, \end{aligned} \quad (6.7)$$

where the Likelihood Ratio Test (LRT) based on the residual received signal is expressed as

$$\text{LRT}''(\mathbf{y}) = \ln \frac{\mathbb{E}_{X_c} [f_{Y|X_r, X_c}(\mathbf{y} | 1, \mathbf{b})]}{\mathbb{E}_{X_c} [f_{Y|X_r, X_c}(\mathbf{y} | 0, \mathbf{b})]}, \quad \mathbf{y} \in \mathbb{C}. \quad (6.8)$$

Then we can plot the ROC curve for the radar system as

$$P_{\text{CD};\text{LRT}''}^*(\epsilon) := \max_{t \in \mathbb{R}: P_{\text{FA};\text{LRT}''}(t) \leq \epsilon} P_{\text{CD};\text{LRT}''}(t). \quad (6.9)$$

Next, the radar symbol estimate is subtracted off the received signal where we have

$$Y'' = Y - |\mathbf{h}_r| \hat{x}_r(Y) = |\mathbf{h}_r| (x_r - \hat{x}_r(Y)) + \mathbf{h}_c x_c + Z,$$

with a likelihood function $f_{Y''|X_c}(y''|b)$ that has no closed form and has to be calculated numerically.

The joint receiver then chooses the transmitted communications symbol as

$$\hat{x}_c(y'') = \arg \max_{b \in \mathcal{X}_c} f_{Y''|X_c}(y''|b), \quad (6.10)$$

from which the communications error rate can be calculated as $\Pr[\hat{x}_c(Y'') \neq x_c | Y'' = y'']$.

Simulating the performance of the aforementioned decoding method is an interesting direction for future work.

APPENDICES

Appendix A

COPYRIGHT PERMISSION

This Appendix includes the copyright permission granted from the IEEE to use published work in thesis. The following statement has been copied from the CopyRight Clearance Center (RightsLink).

Thesis / Dissertation Reuse

The IEEE does not require individuals working on a thesis to obtain a formal reuse license, however, you may print out this statement to be used as a permission grant:

Requirements to be followed when using any portion (e.g., figure, graph, table, or textual material) of an IEEE copyrighted paper in a thesis:

1) In the case of textual material (e.g., using short quotes or referring to the work within these papers) users must give full credit to the original source (author, paper, publication) followed by the IEEE copyright line ©2011 IEEE.

2) In the case of illustrations or tabular material, we require that the copyright line ©[Year of original publication] IEEE appear prominently with each reprinted figure and/or table.

3) If a substantial portion of the original paper is to be used, and if you are not the senior author, also obtain the senior author's approval.

Requirements to be followed when using an entire IEEE copyrighted paper in a thesis:

1) The following IEEE copyright/ credit notice should be placed prominently in the references: ©[year of original publication] IEEE. Reprinted, with permission, from [author names, paper title, IEEE publication title, and month/year of publication]

Appendix A (Continued)

2) Only the accepted version of an IEEE copyrighted paper can be used when posting the paper or your thesis on-line.

3) In placing the thesis on the author's university website, please display the following message in a prominent place on the website: In reference to IEEE copyrighted material which is used with permission in this thesis, the IEEE does not endorse any of [university/educational entity's name goes here]'s products or services. Internal or personal use of this material is permitted. If interested in reprinting/republishing IEEE copyrighted material for advertising or promotional purposes or for creating new collective works for resale or redistribution, please go to http://www.ieee.org/publications_standards/publications/rights/rights_link.html to learn how to obtain a License from RightsLink.

If applicable, University Microfilms and/or ProQuest Library, or the Archives of Canada may supply single copies of the dissertation.

Appendix B

REAL-VALUED PHASE FADING GAUSSIAN CHANNEL AT VERY STRONG RADAR INTERFERENCE

The IC decoder is an approximation of the optimal decoder when $l \gg S \gg 1$ where $\ln I_0(z) \approx z$ for $|z| \gg 1$ and is expressed as

$$\begin{aligned} \hat{\ell}^{(\text{IC})}(\mathbf{y}) &= \arg \min_{\ell \in [1:M]} \left(|\mathbf{y} - \sqrt{S} \mathbf{x}_\ell| - \sqrt{l} \right)^2 \\ &= \arg \min_{\ell \in [1:M]} \left(\frac{|\mathbf{y} - \sqrt{S} \mathbf{x}_\ell|^2 - l}{|\mathbf{y} - \sqrt{S} \mathbf{x}_\ell| + \sqrt{l}} \right)^2. \end{aligned} \quad (\text{B.1})$$

The numerator and the denominator in Equation B.1 can be approximated as

$$\begin{aligned} |\mathbf{y} - \sqrt{S} \mathbf{x}_\ell|^2 - l &= |(\sqrt{S} \mathbf{x} - \sqrt{S} \mathbf{x}_\ell + z) + \sqrt{l} e^{j\Theta}|^2 - l \\ &= |\sqrt{S} \mathbf{x} - \sqrt{S} \mathbf{x}_\ell + z|^2 + 2\sqrt{l} \Re\{e^{-j\Theta}(\sqrt{S} \mathbf{x} - \sqrt{S} \mathbf{x}_\ell + z)\} \\ &= 2\sqrt{l} \left(1 + O(\sqrt{S/l}) \right) \cdot y_{\text{eq}}, \end{aligned} \quad (\text{B.2})$$

$$\begin{aligned} \sqrt{|\mathbf{y} - \sqrt{S} \mathbf{x}_\ell|^2 + l} &= \sqrt{|\sqrt{S} \mathbf{x} - \sqrt{S} \mathbf{x}_\ell + z|^2 + 2\sqrt{l} m' + l + l} \\ &= 2\sqrt{l} \left(1 + \sqrt{|\sqrt{S} \mathbf{x} - \sqrt{S} \mathbf{x}_\ell + z|^2 / l + 2\sqrt{l/l} \Re\{e^{-j\Theta}(\sqrt{S} \mathbf{x} - \sqrt{S} \mathbf{x}_\ell + z)\} + 1} \right) \\ &= 2\sqrt{l} \left(1 + O(\sqrt{S/l}) \right), \end{aligned} \quad (\text{B.3})$$

Appendix B (Continued)

where $O(\cdot)$ denotes the big “O” notation; that is, $f(x) = O(g(x))$ if and only if there exists an x_0 and a positive real number κ such that $|f(x)| \leq \kappa|g(x)|$ for all $x \geq x_0$, and $y_{\text{eq}} := \Re\{e^{-j\Theta}(\sqrt{\mathbf{S}}x - \sqrt{\mathbf{S}}x_\ell + z)\}$. Therefore, by combining Equation B.2 and Equation B.3, we see that at high INR the decoder in Equation B.1 becomes

$$\hat{\ell}^{(\text{IC})}(\mathbf{y}) \triangleq \arg \min_{\ell \in [1:M]} \left(\Re\{e^{-j\Theta}(\mathbf{y} - \sqrt{\mathbf{I}}e^{j\Theta} - \sqrt{\mathbf{S}}x_\ell)\} \right)^2.$$

Appendix C

PROOF OF THE SER FOR A SQUARE M-QAM

A square M-QAM is composed of two symmetric \sqrt{M} -PAM impressed on the in-phase and quadrature carriers. Based on the TIN decoder in Equation 2.7 at low INR, the SER expression of a \sqrt{M} -PAM with half the energy along the real-axis is written as

$$A_{M,S}(\Theta) := 2 \frac{M-1}{M} \left(\frac{1}{2} Q \left(\sqrt{\frac{6S}{M^2-1}} + \sqrt{2I} \cos(\Theta) \right) + \frac{1}{2} Q \left(\sqrt{\frac{6S}{M^2-1}} - \sqrt{2I} \cos(\Theta) \right) \right).$$

Similarly, the SER expression of a \sqrt{M} -PAM with half the energy along the imaginary-axis is written as

$$B_{M,S}(\Theta) := 2 \frac{M-1}{M} \left(\frac{1}{2} Q \left(\sqrt{\frac{6S}{M^2-1}} + \sqrt{2I} \sin(\Theta) \right) + \frac{1}{2} Q \left(\sqrt{\frac{6S}{M^2-1}} - \sqrt{2I} \sin(\Theta) \right) \right).$$

Therefore, conditioned on Θ , the probability of a correct detection for the square M-QAM is the product of correct probabilities for two PAM systems and is given by

$$P_{c,QAM|\Theta} = (1 - A_{\sqrt{M},S/2}(\Theta))(1 - B_{\sqrt{M},S/2}(\Theta)). \quad (\text{C.1})$$

By averaging the expression in Equation C.1 over Θ , the error probability of the TIN decoder is

$$P_{e,QAM}^{(\text{TIN})} = \mathbb{E} [1 - P_{c,QAM|\Theta}] = \mathbb{E}_{\Theta} \left[1 - \left(1 - A_{\sqrt{M},S/2}(\Theta) \right) \left(1 - B_{\sqrt{M},S/2}(\Theta) \right) \right]$$

Appendix C (Continued)

$$= 4 \left(1 - \frac{1}{\sqrt{M}}\right) \mathbb{E}_{\Theta} \left[Q \left(\sqrt{\frac{3S}{M-1}} - \sqrt{2} \cos(\Theta) \right) \right] - \mathbb{E}_{\Theta} \left[A_{\sqrt{M}, S/2}(\Theta) \cdot B_{\sqrt{M}, S/2}(\Theta) \right] \quad (\text{C.2})$$

$$\leq (M-1) \mathbb{E}_{\Theta} \left[Q \left(\sqrt{\frac{3S}{M-1}} - \sqrt{2} \cos(\Theta) \right) \right]. \quad (\text{C.3})$$

The exact SER and its union bound for the square M-QAM are given in Equation C.2 and Equation C.3, respectively.

Appendix D

PROOF OF THE SER FOR A SQUARE M-PSK

For a unit-energy M-PSK, each symbol is defined as

$$x_\ell = e^{j\Theta_\ell} \quad \text{with} \quad \phi_\ell = \frac{2\pi\ell}{M}, \ell \in [1 : M].$$

Therefore, we have the minimum Euclidean distance for an M-PSK as

$$d_{\min} = |x_k - x_\ell| = \left| 2e^{j\frac{\pi+\phi_k+\phi_\ell}{2}} \sin\left(\frac{\phi_k - \phi_\ell}{2}\right) \right| = 2 \sin\left(\frac{\pi}{M}\right).$$

For $l < S$, by the symmetry of the constellation, the error probability for the TIN decoder in Equation 2.7 is

$$P_{e,\text{PSK}}^{(\text{TIN})} = \mathbb{P} \left[\Re\{(\sqrt{l}e^{j\Theta} + Z)e^{-j\frac{\pi+\phi_\ell}{2}}\} \operatorname{sign}\left(\sin\left(\frac{\phi_\ell}{2}\right)\right) > \sqrt{S \sin^2\left(\frac{\phi_\ell}{2}\right)}, \exists \ell \in [1 : M - 1] \right] \quad (\text{D.1})$$

$$\leq (M - 1) \mathbb{E}_\Theta \left[Q \left(\sqrt{2S} \sin\left(\frac{\pi}{M}\right) - \sqrt{2l} \cos(\Theta) \right) \right]. \quad (\text{D.2})$$

The exact SER and its union bound expressions for the M-PSK are given in Equation D.1 and Equation D.2, respectively. Note that further simplifications of the exact SER for the M-PSK in Equation D.1 do not seem possible but this can be done numerically.

Appendix E

SER AND SNR COMPARISON FOR A PAM WITH FIXED NUMBER OF CONSTELLATION POINTS

The SER versus SNR curves for a fixed constellation size M is shown in Figure 7. We consider $M = 2, 4,$ and 8 in this example for the AWGN case ($l = 0$) and the real-valued phase-fading channel case ($l \rightarrow \infty$). Additionally, the designed constellation of size 2 in the high INR regime, marked in dash line, is included for SER and SNR comparison. We see that imposing $\log_{10}(\text{SER}) \leq -3$ results in $M = 2$ at $S_{\text{dB}} \geq 45$, $M = 4$ at $S_{\text{dB}} \geq 55$, and $M = 8$ at $S_{\text{dB}} \geq 63$. Therefore, the proposed constellations yield higher error rates (obviously higher than the tolerable SER in practice) since the range of the SNR used in our constellation design examples in Section 2.6 are quite low.

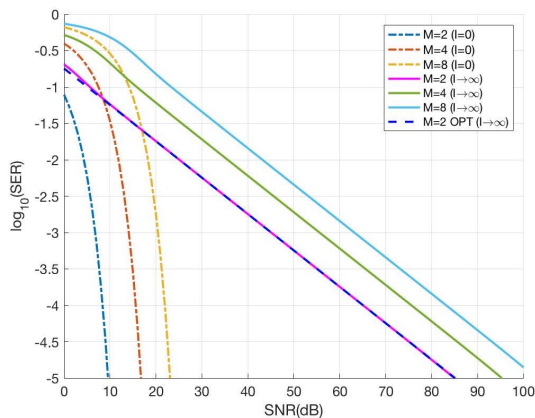


Figure 7: SER comparison vs. S_{dB} for various M values.

CITED LITERATURE

1. Shared spectrum access for radar and communications (ssparc). <http://www.darpa.mil/program/shared-spectrum-access-for-radar-and-communications>.
2. Enhancing access to the radio spectrum (ears). http://www.nsf.gov/funding/pgm_summ.jsp?pims_id=503480.
3. Campbell, R. D.: Radar interference to microwave communication services. Electrical Engineering, 77(10):916–921, October 1958.
4. Wang, H., Johnson, J., Baker, C., Lixin, Y., and Zhang, C.: On spectrum sharing between communications and air traffic control radar systems. In IEEE Radar Conference (RadarConf), pages 1545–1550, May 2015.
5. Wang, L., McGeehan, J., Williams, C., and Doufex, A.: Radar spectrum opportunities for cognitive communications transmission. In International Conference on Cognitive Radio Oriented Wireless Networks and Communications (CROWNCOM), Singapore, May 2008.
6. Bliss, D.: Cooperative radar and communications signaling: The estimation and information theory odd couple. In Proc. of the IEEE Radar Conference (RadarConf), pages 50–55, May 2014.
7. Chiriyath, A., Paul, B., Jacyna, G., and Bliss, D.: Inner bounds on performance of radar and communications co-existence. IEEE Transactions on Signal Processing, 64(2):464–474, January 2016.
8. Hayvaci, H. and Tavli, B.: Spectrum sharing in radar and wireless communication systems: A review. In International Conference on Electromagnetics in Advanced Applications (ICEAA), pages 810–813, August 2014.
9. Antonini, G., Fedele, G., Repaci, P., and Studer, F. A.: Performance comparison of radar receivers subject to amplitude and frequency modulated audio interference. International Radar Conference, pages 233–238, May 1995.
10. Aubry, A., Maio, A. D., Piezzo, M., Naghsh, M. M., Soltanalian, M., and Stoica, P.: Cognitive radar waveform design for spectral coexistence in signal-dependent interference. In Proc. of the the IEEE Radar Conference (RadarConf), pages 474–478, May 2014.

CITED LITERATURE (Continued)

11. Sanders, F. H., Sole, R. L., Bedford, B. L., Franc, D., and Pawlowitz, T.: Effects of rf interference on radar receivers. Technical Report TR-06-444, NTIA, September 2006.
12. Sanders, F. H., Sole, R. L., Carroll, J. E., Secrest, G. S., and Allmon, T. L.: Analysis and resolution of rf interference to radars operating in the band 27002900 mhz from broadband communication transmitters. Technical Report 13-490, NTIA, October 2012.
13. Lackpour, A., Luddy, M., and Wintersm, J.: Overview of interference mitigation techniques between WiMAX networks and ground based radar. In Proc. of the IEEE Wireless and Optical Communication Conference (WOCC), pages 1–5, April 2011.
14. Pasya, I., Mahyuni, A., Adnan, S., and Awang, Z.: Analysis of interference from UWB radar signals on a digital OFDM transmission system. In IEEE International Conference on System Engineering and Technology (ICSET), pages 91–95, June 2011.
15. Cordill, B. D., Seguin, S. A., and Cohen, L.: Radar performance degradation with in-band ofdm communications system interference. US National Committee of URSI National Radio Science Meeting (USNC-URSI NRSM), page 1, January 2013.
16. Deng, H. and Himed, B.: Interference mitigation processing for spectrum-sharing between radar and wireless communications systems. IEEE Transactions on Aerospace and Electronic Systems, pages 1991–1919, July 2014.
17. Cordill, B. D., Seguin, S. A., and Cohen, L.: Electromagnetic interference to radar receivers due to in-band ofdm communications systems. IEEE International Symposium on Electromagnetic Compatibility (EMC), pages 72–75, August 2013.
18. Nartasilpa, N., Tuninetti, D., Devroye, N., and Erricolo, D.: Let's share CommRad: effect of radar interference on an uncoded data communication system. In Proc. of the IEEE Radar Conference (RadarConf), pages 1–5, Philadelphia, PA, May 2016.
19. Nartasilpa, N., Tuninetti, D., Devroye, N., and Erricolo, D.: On the error rate of a communication system suffering from additive radar interference. In Proc. of the IEEE Global Communication Conference (GlobeCom), Washington, DC, December 2016.
20. Shajaiah, H., Khawar, A., Abdel-Hadi, A., and Clancy, T. C.: Resource allocation with carrier aggregation in LTE advanced cellular system sharing spectrum with S-band radar. In IEEE International Symposium on Dynamic Spectrum Access Networks (DYSPAN), April 2014.

CITED LITERATURE (Continued)

21. Zheng, L., Lops, M., Wang, X., and Grossi, E.: Joint design of overlaid communication systems and pulsed radars. IEEE Transactions on Signal Processing, 66(1):139–154, September 2017.
22. Li, B., Kumar, H., and Petropulu, A. P.: A joint design approach for spectrum sharing between radar and communication systems. In IEEE International Conference on Acoustics, Speech and Signal Processing (ICASSP), Shanghai, China, March 2016.
23. Harper, A. D., Reed, J. T., Odom, J. L., Lanterman, A. D., and Ma, X.: Performance of a linear-detector joint radar-communication system in doubly selective channels. In IEEE Transactions on Aerospace and Electronic Systems, April 2017.
24. Zhang, Y., Li, Q., Huang, L., Pan, C., and Song, J.: A modified waveform design for radar-communication integration based on LFM-CPM. In IEEE 85th Vehicular Technology Conference (VTC Spring), Sydney, Australia, June 2017.
25. Dida, M. A., Hao, H., Wang, X., and Ran, T.: Constant envelope chirped OFDM for power-efficient radar communication. In IEEE Information Technology, Networking, Electronic and Automation Control Conference, Chongqing, China, September 2016.
26. Sahin, C., Jakobosky, J., McCormick, P. M., Metcalf, J. G., and Blunt, S. D.: A novel approach for embedding communication symbols into physical radar waveforms. In Proc. of IEEE Radar Conference (RadarConf), Seattle, WA, May 2017.
27. Shi, C., Wang, F., Sellathurai, M., Zhou, J., and Salous, S.: Power minimization based robust OFDM radar waveform design for radar and communication systems in coexistence. IEEE Transactions on Signal Processing, November 2017.
28. Sodagari, S., Khawar, A., Clancy, C., and McGwier, R.: A projection based approach for radar and telecommunication systems coexistence. In Proc. of the IEEE Global Communication Conference (GlobeCom), pages 5010–5014, December 2012.
29. Shajaiah, H., Abdelhadi, A., and Clancy, C.: Spectrum sharing approach between radar and communication systems and its impact on radar’s detectable target parameters. In Proc. of the IEEE 81st Vehicular Technology Conference (VTC Spring), pages 1–6, May 2015.
30. Khawar, A., Abdel-Hadi, A., and Clancy, C.: Spectrum sharing between S-band radar and LTE cellular system: A spatial approach. In IEEE International Symposium on Dynamic Spectrum Access Networks (DYSPAN), pages 7–14, April 2014.

CITED LITERATURE (Continued)

31. H. Zheng, Y. L. and Zhu, Y.: The communication solution for LTE system under radar interference circumstance. International Journal of Antennas and Propagation, 2015, January 2015. Article ID 849695.
32. Heuel, S. and Roessler, A.: Coexistence of s-band radar and 4G mobile networks. In 15th International Radar Symposium (IRS), pages 1–4, June 2014.
33. Babaei, A., Tranter, W. H., and Bose, T.: A practical precoding approach for radar/communications spectrum sharing. In International Conference on Cognitive Radio Oriented Wireless Networks (CROWNCOM), pages 13–18, July 2013.
34. Saruthirathanaworakun, R., Peha, J. M., and Correia, L. M.: Opportunistic sharing between rotating radar and cellular. IEEE Journal on Selected Areas in Communications, 30(10):1900–1910, October 2012.
35. Saruthirathanaworakun, R., Peha, J. M., and Correia, L. M.: Gray-space spectrum sharing between multiple rotating radars and cellular network hotspots. In Proc. of the IEEE 77th Vehicular Technology Conference (VTC Spring), pages 1–5, June 2013.
36. Paul, B., Chiriyath, A. R., and Bliss, D. W.: Joint communications and radar performance bounds under continuous waveform optimization: The waveform awakens. In Proc. of the IEEE Radar Conference (RadarConf), Philadelphia, PA, May 2016.
37. Foschini, G. J., Gitlin, R. D., and Weinstein, S. B.: Optimization of two-dimensional signal constellations in the presence of Gaussian noise. IEEE Transaction on Communications, 22(1):28–38, January 1974.
38. Krishnan, R., Amat, A. G., Eriksson, T., and Colavolpe, G.: Constellation optimization in the presence of strong phase noise. IEEE Transaction on Communications, 61(12):5056–5066, December 2013.
39. Nartasilpa, N., Tuninetti, D., and Devroye, N.: Signal constellation design in the presence of radar interference and Gaussian noise. In Proc. of the IEEE Military Communications Conference (MILCOM), Baltimore, MD, October 2017.
40. Shahi, S., Tuninetti, D., and Devroye, N.: On the capacity of the AWGN channel with additive radar interference. In 54th Annual Allerton Conference on Communication, Control, and Computing, Monticello, IL, September 2016.

CITED LITERATURE (Continued)

41. Nartasilpa, N., Shahi, S., Salim, A., Tuninetti, D., Devroye, N., Erricolo, D., Zilz, D. P., and Bell, M. R.: Let's share CommRad: Co-existing communications and radar systems. In Proc. of IEEE Radar Conference (RadarConf), Oklahoma City, OK, Apr 2018.
42. Bell, M., Devroye, N., Erricolo, D., Koduri, T., Rao, S., and Tuninetti, D.: Results on spectrum sharing between a radar and a communications system. In International Conference on Electromagnetics in Advanced Applications (ICEAA), pages 826–829, Palm Beach, Netherlands Antilles, Aug 2014.
43. Kodituwakku, S., Lamahewa, T., and Dissanayake, T.: Impact on radar probability of detection due to interference from 4g communication signals. In Proc. of IEEE Global Electromagnetic Compatibility Conference (GEMCCON), Adelaide, SA, Australia, Nov 2015.
44. Zilz, D. P. and Bell, M. R.: Statistical modeling of wireless communications interference and its effects on adaptive-threshold radar detection. IEEE Transactions on Aerospace and Electronic Systems, 54(2):890–911, Apr 2018.
45. Richmond, C. and Basu, P.: Architectures for cooperative radar-communications: Average vs. generalized likelihood ratio tests. In Proc. of IEEE Radar Conference (RadarConf), pages 1584–1588, Oklahoma City, OK, Apr 2018.
46. Kay, S. M.: Fundamentals of Statistical Signal Processing: Detection Theory. Prentice Hall, 2 edition, 1998.
47. Heuel, S., McCarthy, D., and Shavit, Y.: Test and measurement of coexistence between S-Band radar and mobile networks. In 2016 26th International Conference Radioelektronika, pages 1–4, April 2016.
48. Goldsmith, A.: Wireless Communications. Cambridge University Press, 2 edition, 2005.
49. Salim, A., Tuninetti, D., Devroye, N., and Erricolo, D.: Modeling the interference of pulsed radar signals in OFDM-based communication systems. In Proc. of the IEEE Radar Conference (RadarConf), Seattle, WA, May 2017.
50. Abramovitz, M. and Stegun, I. A.: Handbook of Mathematical Functions. New York, Dover Publications, Inc, 1970.
51. Ugray, Z., Lasdon, L., Plummer, J., Glover, F., Kelly, J., and Mart, R.: Scatter search and local NLP solvers: a multistart framework for global optimization. INFORMS J. Computing, 19(3):328–340, 2007.

CITED LITERATURE (Continued)

52. Nartasilpa, N., Salim, A., Tuninetti, D., and Devroye, N.: Communications system performance and design in the presence of radar interference. IEEE Transactions on Communications, 66(9):4170–4185, April 2018.
53. Nartasilpa, N., Tuninetti, D., and Devroye, N.: On optimal rocs for a radar system interfered by a communications system. In Proc. of the IEEE International Communications Conference (ICC), 2019.

VITA

Narueporn Nartasilpa

Education	Ph.D. Electrical and Computer Engineering University of Illinois at Chicago, Chicago, Illinois	2014 – 2019
	M.S. Electrical Engineering Florida International University, Miami, Florida	2010 – 2011
	B.E. Electrical Engineering Kasetsart University, Bangkok, Thailand	2004 – 2008
Experience	Wireless Standard Intern at Huawei Technologies, Rolling Meadows, IL USA. Jun 2018 - Aug 2018.	
	Research Assistant at the University of Illinois at Chicago, Chicago, IL USA. Aug 2015 - Dec 2018.	
	Teaching Assistant at the University of Illinois at Chicago, Chicago, IL USA. Sep 2014 - Dec 2018.	
	TIBCO Consultant at Active Enterprise Solutions, Bridgewater, NJ USA. Jul 2012 - May 2013.	
	Research Assistant at Florida International University, Miami, FL USA. Jan 2011 - Aug 2011.	
	Engineer at Advanced Info Service (AIS) Corporation, Bangkok Thailand. Apr 2008 - Jul 2008.	
Publications	N. Nartasilpa , D. Tuninetti and N. Devroye, “On Optimal ROCs for a Radar System Interfered by a Communications System”, (<i>in preparation for</i>) IEEE TCOM 2019.	
	N. Nartasilpa , S. Shahi, A. Salim, D. Tuninetti, N. Devroye, D. Erricolo, D. P. Zilz, and M. R. Bell, “Let’s share CommRad: Co-existing Communications and Radar Systems”, IEEE RadarConf, Oklahoma City, OK, Apr 2018.	
	N. Nartasilpa , D. Tuninetti and N. Devroye, “Communications System Performance and Design in the Presence of Radar Interference”, IEEE Transactions on Communications, vol. 66, no. 9, pp. 4170-4185, Apr 2018.	
	N. Nartasilpa , D. Tuninetti, N. Devroye, and D. Erricolo, “Signal Constellation Optimization in the Presence of Radar Interference and Gaussian Noise”,	

VITA (Continued)

IEEE MILCOM, Baltimore, MD, October 2017.

N. Nartasilpa, D. Tuninetti, N. Devroye, and D. Erricolo, “On the Error Rate of a Communication System Suffering from Additive Radar Interference”, IEEE GLOBECOM, Washington, DC, December 2016.

N. Nartasilpa, D. Tuninetti, N. Devroye, and D. Erricolo, “Let’s share CommRad: Effect of Radar Interference on an Uncoded Data Communication System”, IEEE RadarConf, Philadelphia, PA, May 2016.